frontiers | Frontiers in Earth Science

TYPE Original Research
PUBLISHED 10 August 2023
DOI 10.3389/feart.2023.1243844

OPEN ACCESS

EDITED BY
Fan Yang,
Lanzhou University, China

REVIEWED BY
Qihai Shu,
China University of Geosciences, China
Han Zheng,
Central South University, China
Yuesheng Han,
Beijing Museum of Natural History, China

*CORRESPONDENCE
Ming-Chun Song,
mingchuns@163.com

RECEIVED 21 June 2023
ACCEPTED 01 August 2023
PUBLISHED 10 August 2023

CITATION
Li J, Dai C-G, Wang C-W, Song M-C, Wang C-J, Li S-Y, Wang R-S, Shi H-J, Xu K-L and Wang P (2023), Possible genetic relationship between Mesozoic magmatic rocks and gold mineralization in the Jiaodong Peninsula (Eastern China): constraints of magmatic evolution and physicochemical conditions.
Front. Earth Sci. 11:1243844.
doi: 10.3389/feart.2023.1243844

Possible genetic relationship between Mesozoic magmatic rocks and gold mineralization in the Jiaodong Peninsula (Eastern China): constraints of magmatic evolution and physicochemical conditions

Jian Li[1,2,3], Chang-Guo Dai[4], Chang-Wei Wang[1,3], Ming-Chun Song[5]*, Chang-Jiang Wang[1,3], Shi-Yong Li[5], Run-Sheng Wang[6], Hong-Jiang Shi[4], Kai-Lei Xu[4] and Ping Wang[4]

[1]School of Resources and Environmental Engineering, Shandong University of Technology, Zibo, China, [2]Institute of Geology, Chinese Academy of Geological Sciences, Beijing, China, [3]Shandong Zhengyuan Geological Resources Exploration Co., Ltd., Zibo, China, [4]Shandong Province Nuclear Industry Geological Group 273, Yantai, China, [5]Hebei Province Collaborative Innovation Center for Strategic Critical Mineral Research, Hebei GEO University, Shijiazhuang, China, [6]Shandong Institute of Geophysical and Geochemical Exploration, Ji'nan, China

The Jiaodong Peninsula is China's largest gold province and the third largest in the world. Although gold mineralization is associated with Mesozoic granites temporally and spatially, the specific genetic association remains unclear, leading to ambiguity regarding the genetic type of gold deposits. To address this issue, we conducted whole-rock major and trace elements, LA–ICP–MS zircon U–Pb geochronology and trace elements geochemical analyses on the Linglong (Linglong suite), Yashan, and Nansu (Weideshan suite) plutons, and compiled contemporaneous magmatic rock data. Our results show that the granites were emplaced at 161 ± 2, 118 ± 1, and 121 ± 2 Ma, respectively. Geochemically, these rocks exhibit high Al_2O_3 (12.73–14.10 wt%) content and Sr/Y (35.54–136.50) ratio, and low Y (3.26–11.20 ppm) and Yb (0.33–0.97 ppm) contents, indicating the adakitic rock properties. They were formed through partial melting of the thickened lower crust associated with subduction of the paleo-Pacific Plate. The Early Cretaceous granites contain a large amount of mafic microgranular enclaves, indicating the presence of mantle material mixing in the source area. Zircon trace elements show that the pre-mineralization magma (Linglong) had relatively low oxygen fugacity and temperature (ΔFMQ = −2.5 to +1.9, T-Ti in zircon (mean) = 740°C) compared to the mineralization magma (ΔFMQ = +0.5 to +3.9, T-Ti in zircon (mean) = 755°C). The physicochemical conditions in the pre-mineralization magma source area may be favorable for sulfide accumulation (may including gold). During the Early Cretaceous, North China Craton decratonization reached its climax, and a large number of adakitic crust-mantle mixed oxidized magma upwells, allowing for the migration and mineralization of a large amount of sulfides and gold. This model helps explain the transient, explosive, and genetic categories in Jiaodong gold deposits.

KEYWORDS

adakitic rocks, thickened lower crust, oxygen states, Jiaodong gold deposits, North China craton

1 Introduction

The North China Craton (NCC) is an ancient cratonic blocks in Eastern Asia, comprising Archean to Paleoproterozoic basement rocks (Figure 1A) (Hart et al., 2002; Nie et al., 2004; Santosh, 2010; Zhao and Zhai, 2013). Unlike traditional cratons, the NCC experienced extensive magmatism and tectonism in the Triassic and reaching its peak during the Early Cretaceous due to the roll-back of the paleo-Pacific Plate, a process known as decratonization (Gao et al., 2002; Wu et al., 2008; Zhu et al., 2015; Li et al., 2020a; Yang et al., 2021). This process resulted in large-scale mineralization events, with gold mineralization being the most typical. The Jiaodong Peninsula has the largest gold mineralization scale, accounting for 40% of the total gold deposits in China, with over 200 small, medium, and large gold deposits formed at 125–115 Ma (Yang et al., 2014; Fan et al., 2016; Song et al., 2018; Deng et al., 2020; Song et al., 2020; Song et al., 2021), characterized by explosive mineralization (formation >5,000 t gold in a short duration). Furthermore, 80% of gold deposits are hosted in granite (Song et al., 2018) (Supplementary Figure S1), with a significant portion of

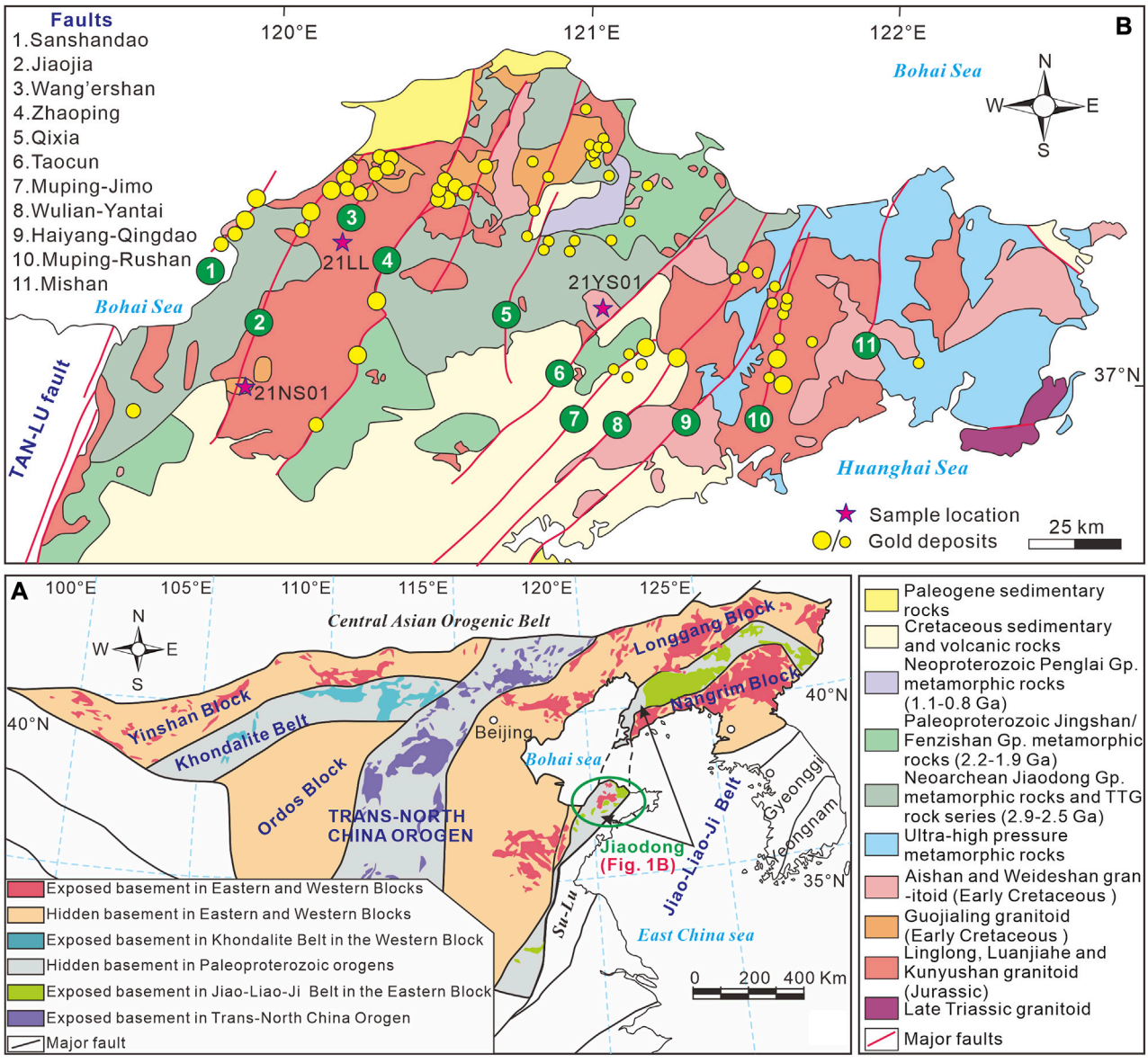

FIGURE 1
(A) The distribution of the Archean to Paleoproterozoic basement rocks in the NCC (Zhao et al., 2005); **(B)** Sketch geologic map of the Jiaodong Peninsula (after Song et al., 2020).

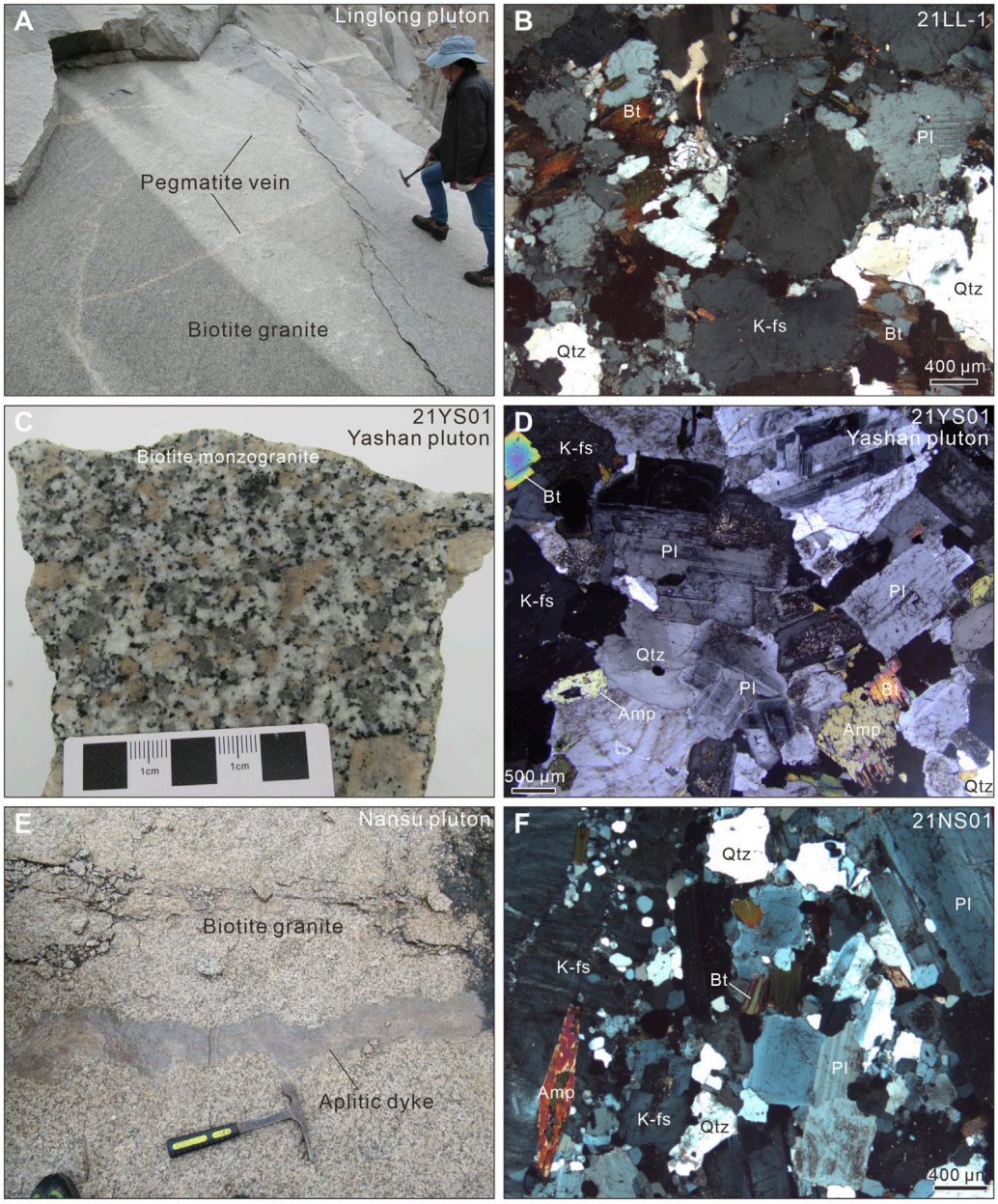

FIGURE 2
Photographs and microphotographs (cross-polarized light) of the studied samples. **(A,B)** biotite granite (Linglong suite); **(C,D)** biotite monzogranite (Yashan pluton); **(E,F)** biotite granite (Nansu pluton). Abbreviation: Amp, amphibole; Bi, Biotite; K-fs, Potassium feldspar; Pl, Plagioclase; Qtz, Quartz.

these granites are coeval with the gold mineralization. However, the relationship between explosive gold mineralization and large-scale magmatism induced by the decratonization process remains controversial, with scholars debating whether these magmatic rocks provided direct material, heat, or water for the formation of gold mineralization (Ma et al., 2014; Deng et al., 2020; Zhang et al., 2020; Dong et al., 2023a; Dong et al., 2023b; Dong et al., 2023c). Current studies have mostly focused on the mineralization itself and less on the physicochemical conditions of the magma, which has limited our understanding of ore genesis and exploration work. Additionally, changes in mantle composition and oxygen fugacity during the transition from compression to an extensional environment from the Jurassic to Cretaceous may have restricted key indicators of gold formation.

To better understand the constraints of Mesozoic magmatic rocks on the formation of gold mineralization in the Jiaodong Peninsula, we present petrographic observations, whole-rock major and trace element geochemistry data, and Laser ablation inductively coupled plasma mass spectrometry (LA–ICP–MS) U–Pb dating of zircon ages and trace elements for representative granites from Jiaodong Peninsula. These data provide new insights about the origin and petrogenesis of these Mesozoic granitic rocks within the Jiaodong Peninsula and yield important changes in key parameters that may constrain gold mineralization.

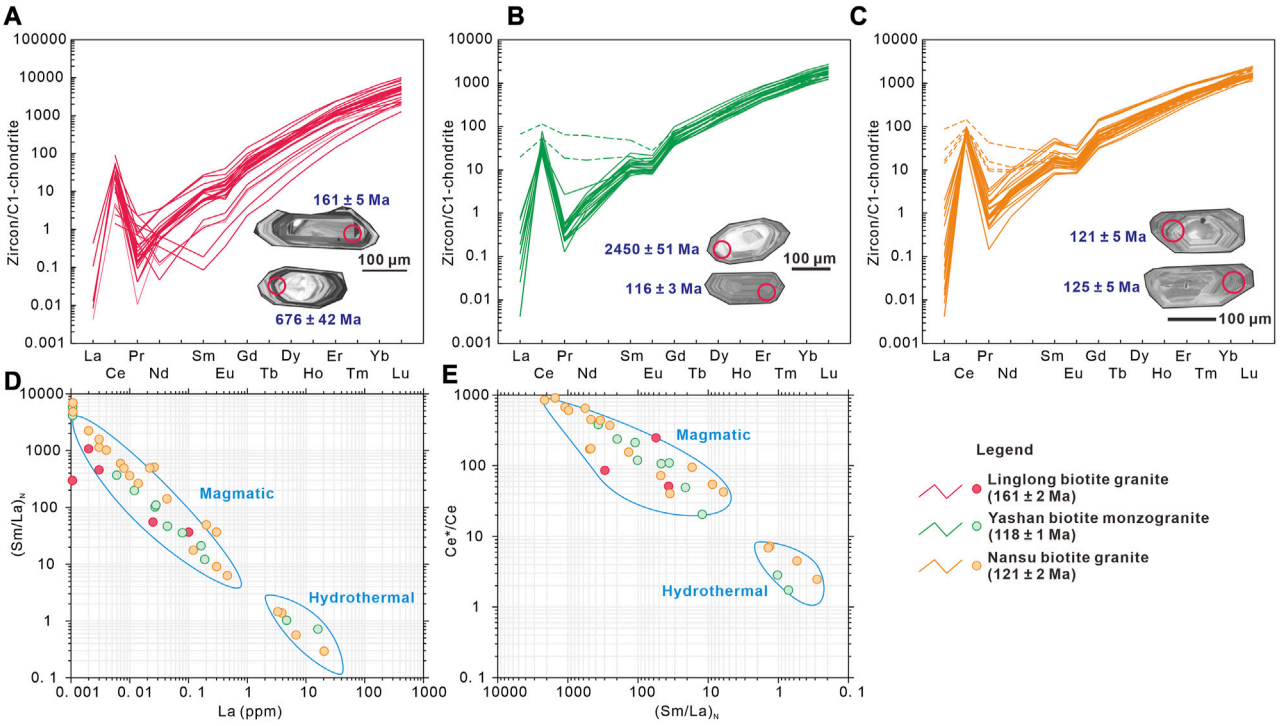

FIGURE 3
(A–C) Chondrite-normalized rare earth element patterns (normalizing values are from McDonough and Sun, 1995) and showing representative CL images (LREE-enrichment patterns (dashed lines in the figure), which may be contaminated by mineral/melt inclusions; as suggested by Zhong et al. (2019); Cai et al. (2021)); **(D)** $(Sm/La)_N$ vs. La; **(E)** Ce/Ce* vs. $(Sm/La)_N$ diagrams (the range of "magmatic" and "hydrothermal" is based on Hoskin, 2005) of zircons from the Jiaodong Peninsula Mesozoic granitoids.

2 Geological setting

The North China Craton (NCC) is the largest and oldest craton in China, covering approximately 1.5 million square kilometers and dating back to at least 3.8 billion years (Figure 1A) (Liu et al., 1992; Zhao et al., 2005). It consists of Archean-Paleoproterozoic basement and Mesoproterozoic-Cenozoic volcanic-sedimentary sequences (Santosh, 2010; Zhao and Zhai, 2013; Yang et al., 2018; Yang et al., 2020) and was formed by the combination of the western (Yinshan and Ordos blocks at ~1.95 Ga along the khondalite Belt) and eastern blocks (Longgang and Nangrim blocks at ~1.95 Ga along the Jiao-Liao-Ji Belt) along the Trans-North China Orogen (~1.85 Ga) (Figure 1A; Zhao et al., 2001; Zhao et al., 2005). The NCC remains stable (lack of earthquakes, tectonism, and magmatism) after cratonization, and the decratonization occurred until the Mesozoic. Significant tectonic-thermal events occurred mainly in the east of NCC, including the Jiaodong and Liaodong peninsulas (Li et al., 2019a; Li et al., 2020a; Li et al., 2020b; Li et al., 2023a; Li et al., 2023b). Unlike conventional cratons, the Mesozoic magmatism has significantly changed the crust thickness, nature, and isotope composition of NCC (i.e., decratonization) (Menzies et al., 1993; Griffin et al., 1998; Yang et al., 2021), which is also accompanied by gold mineralization in Jiaodong Peninsula (Figure 1B).

The Jiaodong Peninsula is the largest gold province in China (>5,000 t), and is the third largest in the world after the Witwatersrand Basin (South Africa) and the Muruntau district (Uzbekistan) (Song et al., 2021). It mainly consists of Precambrian crystalline basement, Mesozoic-Cenozoic volcanic-sedimentary rocks, and intrusive rocks (Figure 1B). The Precambrian meta-sedimentary rock series mainly includes Neoarchean Jiaodong Group, Paleoproterozoic Jingshan Group, Fenzishan Group, and Neoproterozoic Penglai Group (Figure 1B) (Li et al., 2022). Faults are mainly distributed along the NE-NNE-striking of the Jiaodong Peninsula, with NNE-striking faults playing a significant role as the main ore-controlling structures (Figure 1B). The strong Mesozoic magmatism in the Jiaodong is mainly concentrated in the Jurassic and Early Cretaceous. Jurassic intrusions mainly include Linglong, Luanjiahe, and Kunyushan, mainly composed of granite, granodiorite, and monzogranite, formed at 170–150 Ma (Yang et al., 2012; Ma et al., 2013; Yang et al., 2017; Wang et al., 2022; Dong et al., 2023a). The early Cretaceous intrusions are composed of Guojialing (130–127 Ma; Yang et al., 2012; Jiang et al., 2016; Dong et al., 2023a), Weideshan (125–110 Ma; Goss et al., 2010; Li et al., 2012; Song et al., 2020; Dong et al., 2023a; Dong et al., 2023b; Dong et al., 2023c), and Laoshan (125–108 Ma; Goss et al., 2010; Wang et al., 2021; Wang et al., 2023) suites, mainly composed of granodiorite, monzogranite, and syenite (Figure 1B). The Mesozoic volcanic rocks are mainly distributed in the Jiaolai basin, consisting of Qingshan, Wangshi, and Laiyang Groups, including rhyolite, andesite, dacite, and tuff (Dong et al., 2023a). Gold deposits are mainly found in magmatic rocks and are distributed along NNE-striking faults (Figure 1B).

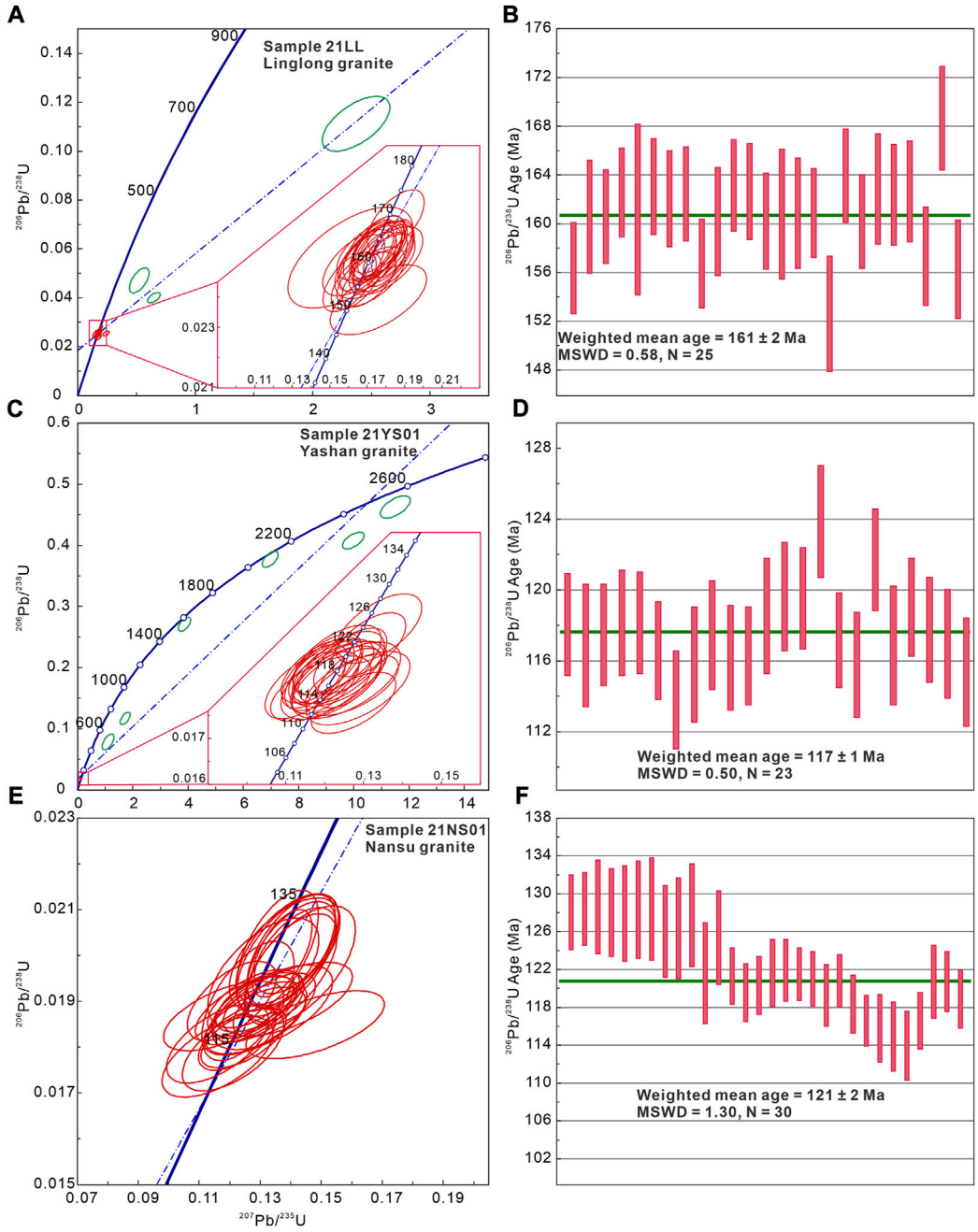

FIGURE 4
Zircon U-Pb concordia **(A, C, E)** and weighted mean $^{238}U/^{206}Pb$ ages **(B, D, F)** of the Jiaodong Peninsula Mesozoic granitoids. Green ellipses represent inherited zircon.

3 Sample description

In this study, we collected samples from the Cuizhao unit of Linglong suite, Yashan and Nansu plutons of Weideshan suite.

3.1 Linglong suite

The Cuizhao unit (biotite granite) of the Linglong suite collected in this study is located in the west of Zhaoyuan City, Shandong Province (labeled as 21LL; sample location: N 37°23′28.5″, E 120°10′21.3″; Figure 1B). The biotite granite shows the obvious gneissic structure (mineral orientation arrangement) and develops pegmatite vein (Figure 2A). The biotite granite is mainly composed of quartz (25%–30%), plagioclase (35%–40%), potassium feldspar (15%–20%), and biotite (~10%), and a small amount of apatite, zircon, and sphene accessory minerals (~1%) (Figure 2B). Apatite is mainly needle columnar, distributed in plagioclase, and formed later than plagioclase. Amphibole is not developed in the dark minerals of the whole Linglong suite, which is different from the Early Cretaceous suite.

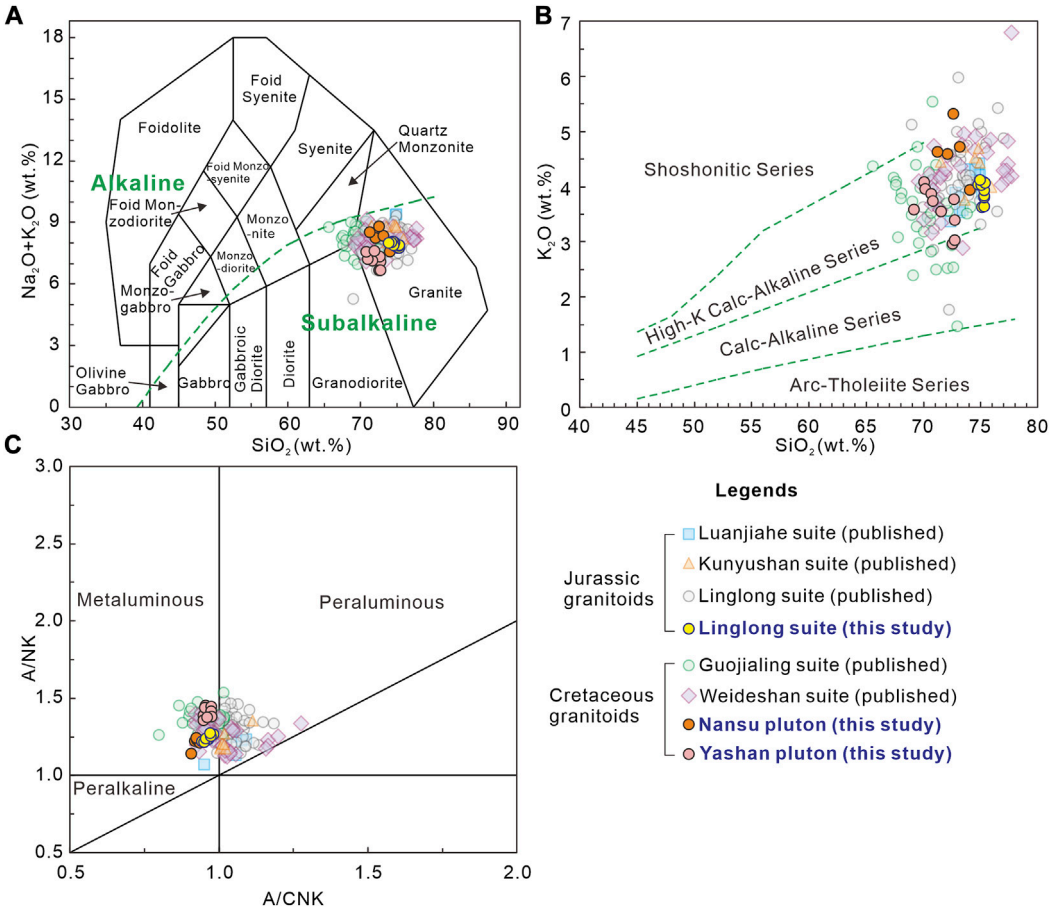

FIGURE 5
Whole-rock geochemistry plots for the Jiaodong Peninsula Mesozoic granitoids. **(A)** Total alkalis ($Na_2O + K_2O$) vs. silica (SiO_2) (Irvine and Baragar, 1971); **(B)** K_2O vs. SiO_2 (Peccerillo and Taylor, 1976); **(C)** A/NK vs. A/CNK (Maniar and Piccoli, 1989). Published data are from Hou et al., 2007; Li et al., 2012; Yang et al., 2012; Ma et al., 2013; Li et al., 2019b; He, 2021; Wang et al., 2021; Dong et al., 2023a, Dong et al., 2023b.

3.2 Weideshan suite

3.2.1 Yashan pluton

The Yashan pluton (biotite monzogranite) in this study belongs to Weideshan suite, which is located in Qixia City, Shandong Province (labeled as 21YS01; sample location: N 37°03′42.5″, E 121°09′48.7″; Figure 1B). The biotite monzogranite is mainly composed of quartz (30%–35%), plagioclase (30%–35%), potassium feldspar (25%–30%), biotite (~10%), and amphibole (5%–10%), and the accessory minerals are apatite and sphene (~1%) (Figures 2C, D). The oscillatory zone and polycrystalline twins of plagioclase are relatively developed (Figure 2D).

3.2.2 Nansu pluton

The Nansu pluton (biotite granite) in this study also belongs to the Weideshan suite, collected from the south of Laizhou City, Shandong Province (labeled as 21NS01; sample location: N 37°00′21.5″, E 119°58′55.3″; Figure 1B). Nansu biotite granite has medium-coarse grain structure and develops aplitic dyke (Figure 2E). Mineral assemblages are mainly quartz (30%–35%), plagioclase (35%–40%), potassium feldspar (20%–25%), biotite (~10%), and amphibole (5%–10%), and apatite and zircon accessory minerals (Figure 2F).

4 Analytical methods

4.1 Zircon U–Pb dating and trace elements

Zircon grains were separated from these samples by traditional magnetic and heavy liquid technology, and finally handpicked in Guangzhou Tuoyan Analytical Technology Co., Ltd. (Guangzhou, China) using a binocular microscope. Transmission, reflected light, and cathodoluminescence (CL) images were collected to reveal the internal textures and surface characteristics of zircon. Zircon U–Pb age and *in situ* trace element content analyses were completed by the Institute of Geology, Chinese Academy of Geological Sciences using Laser ablation inductively coupled plasma mass spectrometry (LA–ICP–MS) (193 nm LA system and Agilent 7900 ICP-MS instrument). During the test, the spot size is 30 μm, the energy is 2 J/cm^2, and the repetition rate is 5 Hz.

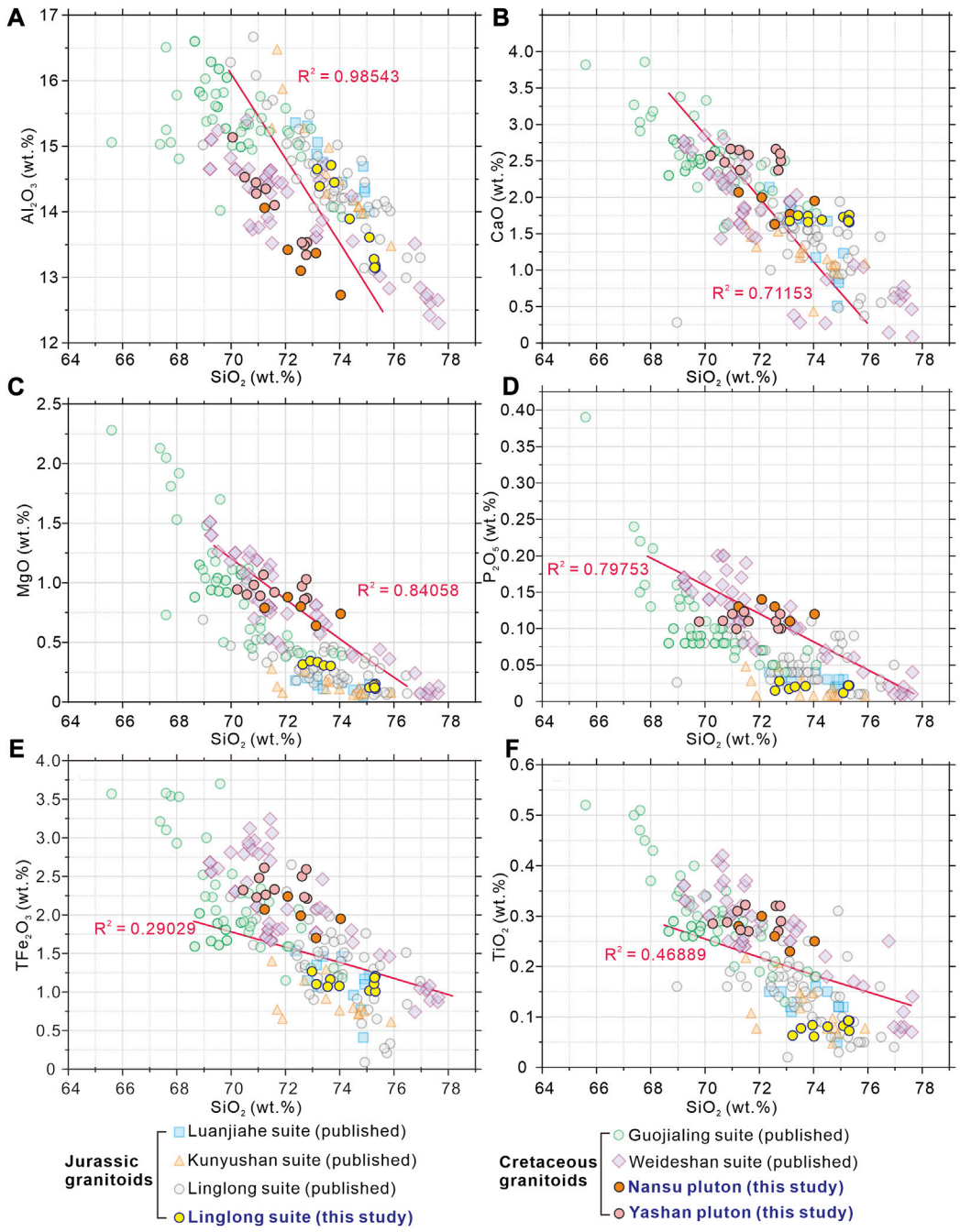

FIGURE 6
Major element Harker variation diagrams of the Mesozoic granitoids from the Jiaodong Peninsula. The published data is the same as in Figure 5.

Zircon 91500 (1062.4 ± 7.7 Ma; n = 34) is used as an external standard, and NIST 610 glass (1388 ± 12 Ma; n = 17) and SA01 (533.7 ± 5.3 Ma; n = 17) is used to calibrate the age and trace elements (analysis two 91500 standard samples and one SA01 standard sample at every 10 sample points). Typically, a gas blank of 20s is collected and a signal interval of 35–40s is processed for data processing, followed by deep fractionation correction using an exponential equation (Paton et al., 2010), and the Isoplot program (Ludwig, 2003) was used to obtain the concordia and weighted diagrams. Common Pb was corrected following the method described by Andersen (2002).

4.2 Whole-rock major and trace element analyses

In this study, we have determined twenty-five major elements and fifteen trace elements of the three plutons above, all of which

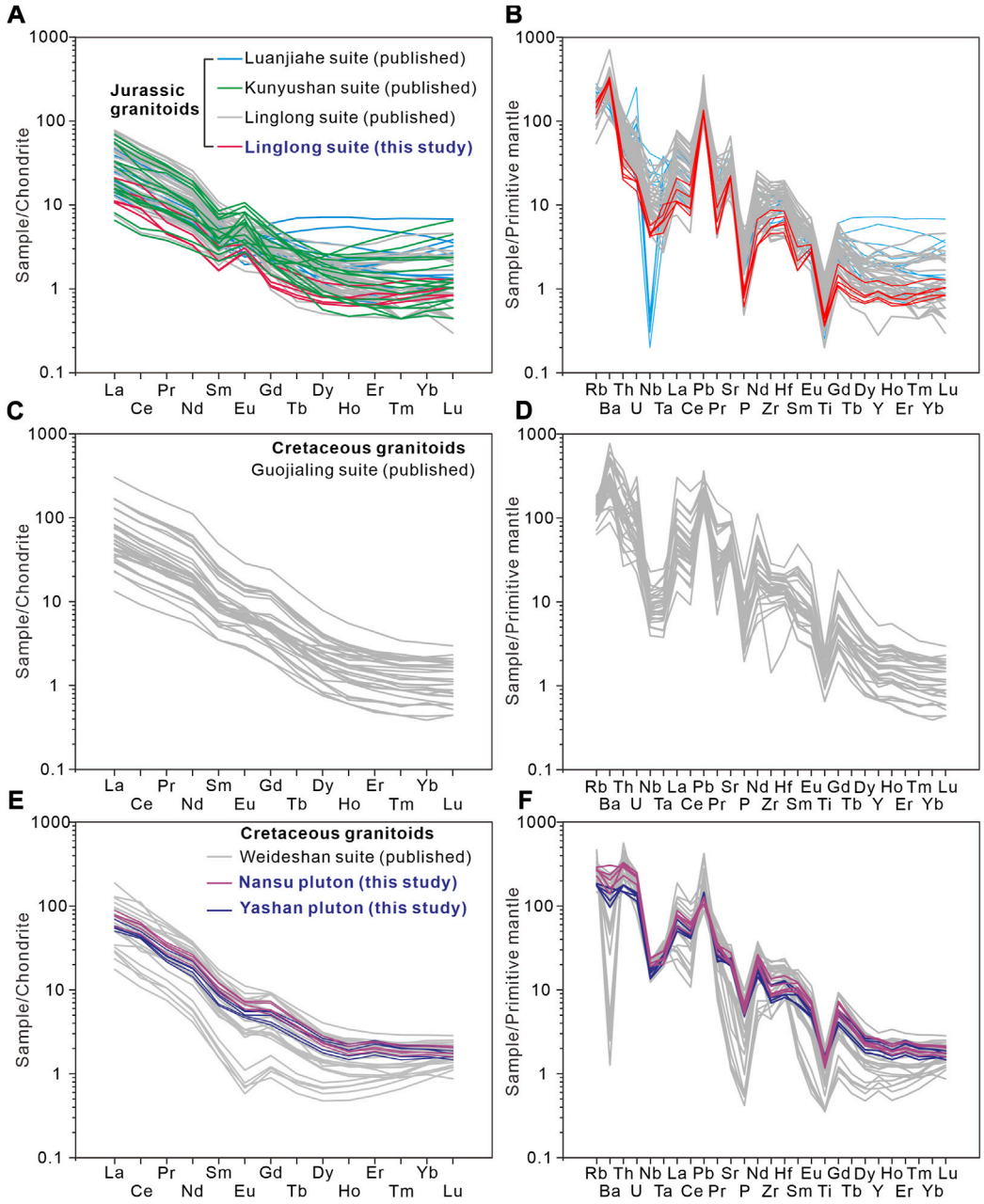

FIGURE 7
Chondrite-normalized REE patterns **(A,C,E)** and primitive mantle-normalized trace element variation diagrams **(B,D,F)** for the Jiaodong Peninsula Mesozoic granitoids. Normalizing values are from McDonough and Sun (1995). The published data is the same as in Figure 5.

were completed in Guangzhou Tuoyan Analytical Technology Co., Ltd. The whole-rock major elements are completed by Primus II X-ray fluorescence spectrometer (XRF). Burn in a 1,000 °C muffle furnace for 2 h, and calculate the loss on ignition (LOI) after cooling. Take a 0.6 g sample and place it in an 1150°C sample melting furnace (14 min), and conduct XRF test after cooling. The whole-rock trace elements are completed by the Semeferri CAP RQ system. During the test, OU-6, BCR-1, and GBPG-1 were used as standard samples to monitor the accuracy of data results, and the RSD of data results was better than 5%.

5 Results

5.1 Zircon U–Pb ages and trace elements

Three magmatic rock samples were analyzed for zircon U–Pb ages and trace elements, and the results are presented in Figures 3, 4 and Supplementary Table S1.

5.1.1 Linglong biotite granite (sample 21LL)

The zircon grains of this sample have clear oscillatory zones, containing some mineral inclusions, 120–400 μm in length and

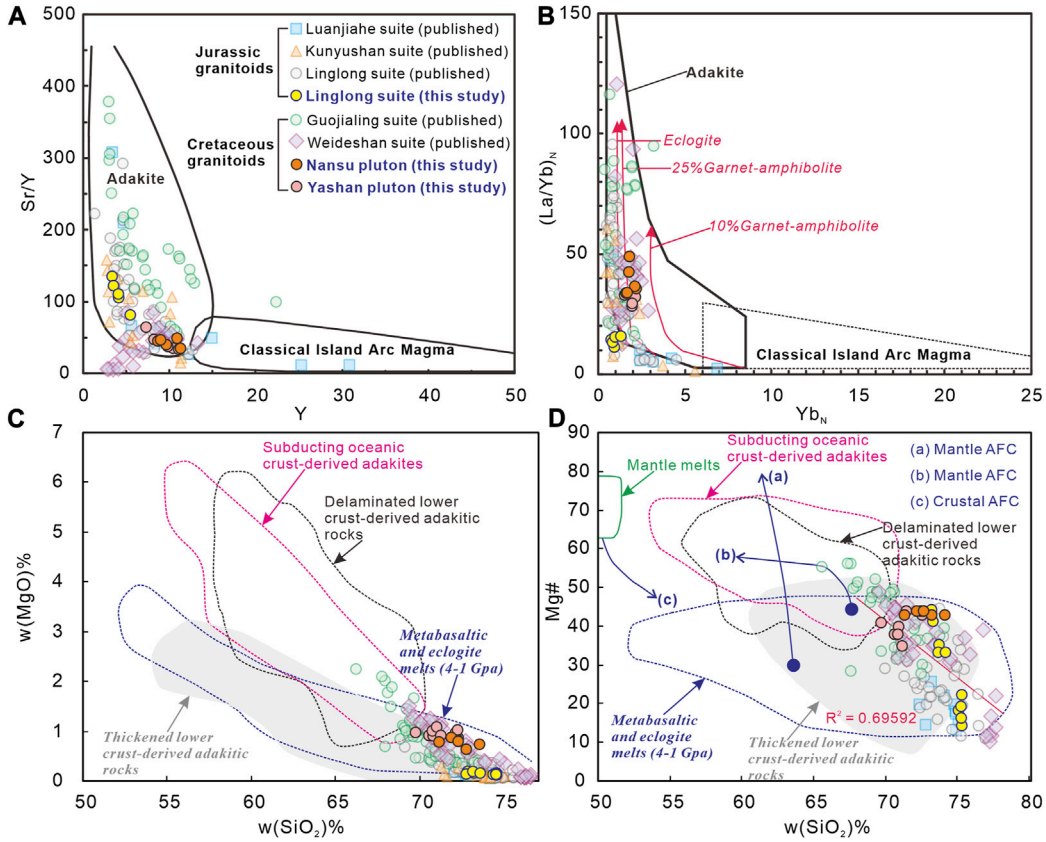

FIGURE 8
(A) Sr/Y vs. Y (after Martin, 1986; Defant and Drummond, 1990); **(B)** $(La/Yb)_N$ vs. Yb_N (after Martin, 1987; Drummond et al., 1996; Martin et al., 2005); **(C)**. MgO vs. SiO_2; **(D)**. Mg# vs. SiO_2 of the various magmatic phases from Jiaodong Peninsula. Data sources are as in Figure 5.

40–120 μm in width (Figure 3A). The composition of REEs in zircon shows significant positive Ce anomalies (Ce/Ce* = 1.73–1583.58) (Figure 3A), combined with a high Th/U ratio (0.01–0.91), indicating that these are all magmatic zircons (Figures 3D, E) (Hoskin and Black, 2000; Rubatto and Gebauer, 2000; Hoskin, 2005). There are 30 zircons analyzed, of which 5 points deviate significantly from the concordia line and may be inherited zircons (296 ± 21 Ma, 252 ± 9 Ma, 676 ± 42 Ma, 162 ± 4 Ma, and 177 ± 4 Ma) (Supplementary Table S1), the remaining 25 data are concentrated at 169 ± 4 Ma to 152 ± 5 Ma, with a weighted mean $^{206}Pb/^{238}U$ age of 161 ± 2 Ma (Figures 4A, B).

5.1.2 Yanshan biotite monzogranite (sample 21YS01)

The zircon of this sample is generally dark gray color with significant oscillatory domains and contains a few mineral inclusions, 80–220 μm in length and 40–100 μm in width (Figure 3B). The REE distribution pattern and the high Th/U ratio (0.02–0.92) of zircon indicate that these are mainly of magmatic origin, some of which are in the hydrothermal range and may be related to mineral inclusions (Figures 3D, E). Thirty zircon grains were analyzed, seven of which deviated significantly from the concordia line and may be inherited zircons (1543 ± 39 Ma, 2061 ± 41 Ma, 207 ± 6.2 Ma, 709 ± 39 Ma, 481 ± 52 Ma, 2204 ± 41 Ma, and 2450 ± 51 Ma), while the remaining 23 zircon $^{206}Pb/^{238}U$ ages were concentrated in the range of 124 ± 3 Ma to 114 ± 3 Ma, with a weighted mean $^{206}Pb/^{238}U$ age of 118 ± 1 Ma (Figures 4C, D).

5.1.3 Nansu biotite granite (sample 21NS01)

The zircon grains in this sample are gray and contain mineral inclusions, with a length of 60–300 μm and a width of 50–100 μm (Figure 3C). The REE distribution pattern and high Th/U ratio (0.29–1.25) of zircon also indicate magmatic origin (Figures 3D, E). The 30 zircon grains analyzed contain no captured/inherited zircons, with $^{206}Pb/^{238}U$ ages concentrated in the range 129 ± 5 Ma to 114 ± 4 Ma and a weighted mean age of 121 ± 2 Ma (Figures 4E, F).

5.2 Whole-rock major and trace element geochemistry

The whole-rock geochemical data are shown in Figures 5–7 and Supplementary Table S2. Overall, the magmatic rocks in this study all have high SiO_2 (69.81–75.32 wt%), Na_2O (3.48–4.18 wt %), and K_2O (2.97–5.32 wt%) contents. In the total alkali (Na_2O + K_2O) vs. SiO_2 diagram, these magmatic rocks fall into the granite range of the subalkaline series (Figure 5A). They belong to the high-K calc-alkaline series in the plot of SiO_2 vs. K_2O diagram (Figure 5B) (except for one high-K sample from the Nansu

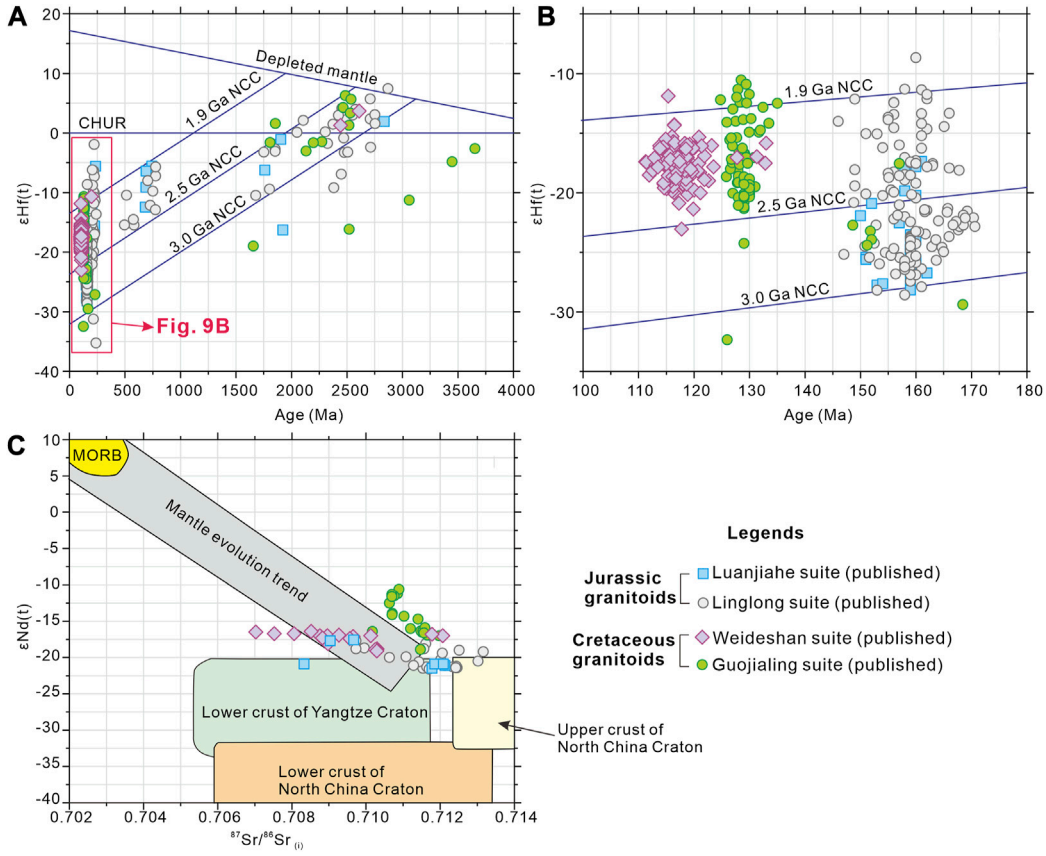

FIGURE 9
The εHf(t) vs. U–Pb age (Ma) **(A,B)** and plots of εNd(t) vs. $(^{87}Sr/^{86}Sr)_i$ ratio **(C)** diagrams for the granites from the Jiaodong Peninsula. Data sources are as in Figure 5.

pluton). Their A/CNK [molar $Al_2O_3/(CaO + K_2O + Na_2O)$] values are all <1 (0.91–0.99), indicating the characteristics of metaluminous in the A/CNK vs. A/NK diagram (Figure 5C). In Harker diagram, the correlation between SiO_2 vs. Al_2O_3, CaO, MgO, P_2O_5, TFe_2O_3, and TiO_2 (Figure 6) is significant (especially adding published data), indicating the crystallization differentiation of minerals.

In the composition of rare earth elements (REE), these magmatic rocks have the characteristics of enriched LREE and depleted HREE (Figures 7A, C, E). However, there are significant differences between the total REE and Eu anomalies. The total REE of the Jurassic Linglong granite is low (28.01–58.25 ppm) and shows positive Eu anomalies (Eu/Eu* = 1.45–2.27), while the Cretaceous Weideshan suite has a high total REE (132.87–213.19 ppm) and negative Eu anomalies (Eu/Eu* = 0.83–1.01) (Supplementary Table S2). Published literature also shows such differences (e.g., Dong et al., 2023a). In the trace element spider diagrams, all samples are enriched in large-ion lithophile elements (LILEs; e.g., Rb and Pb) and depleted in high-field-strength elements (HFSEs; e.g., Nb, Ta, and Ti) and P. In addition, some elements are different. The Linglong and Guojialing suites are enriched in Ba and Sr, while the Weideshan suite shows the characteristics of depletion, suggesting differences in the fractionation of potassium feldspar.

6 Discussion

6.1 Petrogenesis

6.1.1 Source characteristics of adakitic rocks

The Mesozoic granitoids in the Jiaodong Peninsula exhibit high Al_2O_3 (12.73–14.10 wt%) content, Sr/Y (35.54–136.50), and $(La/Yb)_N$ (11.42–48.90) ratios, as well as low Y (3.26–11.20 ppm) and Yb (0.33–0.97 ppm) contents. These characteristics suggest that they are adakitic rocks (Defant and Drummond, 1990; Martin, 1999; Martin et al., 2005; Richards and Kerrich, 2007; Moyen, 2009). The Sr/Y vs. Y and $(La/Yb)_N$ vs. Yb_N discrimination diagrams also support this conclusion (Figures 8A, B). However, the Mesozoic granites in Jiaodong have a large range variation of these elements/ratios, and some of them fall within the range of island arc magma (Figures 8A, B), similar to transitional properties (e.g., Cai et al., 2021), which may be due to different magmatic processes. Therefore, the term "adakitic rocks" (or "adakite-like rocks") is used here to introduce adakites, as proposed by Richards and Kerrich (2007).

Adakitic rocks can be formed through various processes, including: 1) partial melting of the delaminated lower crust (Xu et al., 2002); 2) partial melting of subducted oceanic slabs (Defant and Drummond, 1990; Stern and Kilian, 1996; Martin, 1999;

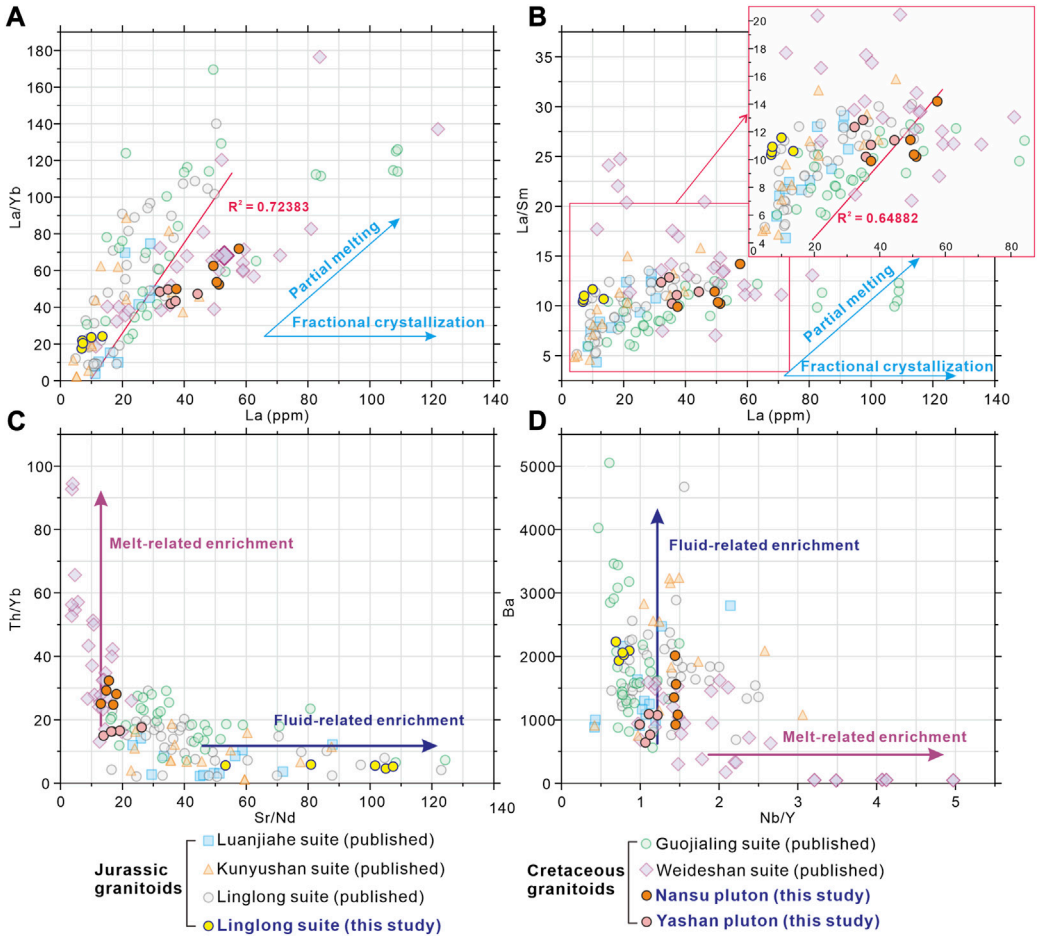

FIGURE 10
Plots of **(A)** La vs. La/Yb, **(B)** La vs. La/Sm, **(C)** Sr/Nd vs. Th/Yb (Woodhead et al., 1998), and **(D)** Nb/Y vs. Ba (Kepezhinskas et al., 1997) for the Mesozoic granites from Jiaodong Peninsula.

Smithies, 2000; Defant et al., 2002); 3) assimilation and fractional crystallization (AFC) of basaltic magmas, or mixing with such magma (Castillo et al., 1999; Macpherson et al., 2006); 4) Partial melting of thickened lower crustal material (Atherton and Petford, 1993; Stevenson et al., 2006). High Mg# value, Co, and Ni contents are commonly found in the source areas of the delaminated lower crust and subducted oceanic slabs. However, the Mg# values and Co and Ni contents of the Jurassic Linglong and Cretaceous Weideshan granites studied in this study are both at a lower level (Supplementary Table S2), especially for the Linglong granites, which have a Mg# value of only 14–22, probably from partial melting of crust derived materials. A large number of dioritic xenoliths–enclaves have been found in previous studies of Weideshan suite (e.g., Song et al., 2020; Song et al., 2021), suggesting that magma mixing or the injection of mafic magma has a certain source contribution. This may also be the reason why the Nansu and Yashan plutons have medium Mg# (43–44). It is shown in SiO_2 (wt%) *versus* MgO (wt%) and Mg# diagram that these points in this study also fall within the partial melting range of thickened lower crustal material (Figures 8C, D). The data in the literature also shows such characteristics. In addition, some characteristic trace element ratios also indicate that these rocks are mainly crustal-derived, because these rocks have: 1) average Zr/Hf (33.7) and Nb/Ta (13.0) ratios similar to the average crustal values (33 and 11.4, respectively; Taylor and McLennan, 1985; Rudnick et al., 2004), but lower than the primitive mantle values (37 and 17.8, respectively; McDonough and Sun, 1995); 2) average Ce/Pb (3.3) and Nb/U (5.0) ratios that reflect a continental crustal source (4 and 10; Hofmann et al., 1986); 3) average Rb/Sr (0.3), Ti/Zr (14.2) and Ti/Y (161.5) ratios similar to typical crustal-derived magma (Pearce, 1983; Tischendorf and Paelchen, 1985; Wilson, 1989). Therefore, the Mesozoic adakitic rocks in the Jiaodong Peninsula originated from the partial melting of thickened lower crustal material, and the Cretaceous granite may also be accompanied by the injection process of mafic magma. This conclusion is supported by a large number of Sr-Nd-Hf isotope analyses conducted by previous studies (Figure 9). The Cretaceous granites are located in/near the mantle evolution trend range (Figure 9C). The Jurassic granites are more derived from ancient crustal components, while the Cretaceous Guojialing and Weideshan granites show a higher involvement of mantle components (Figure 9C).

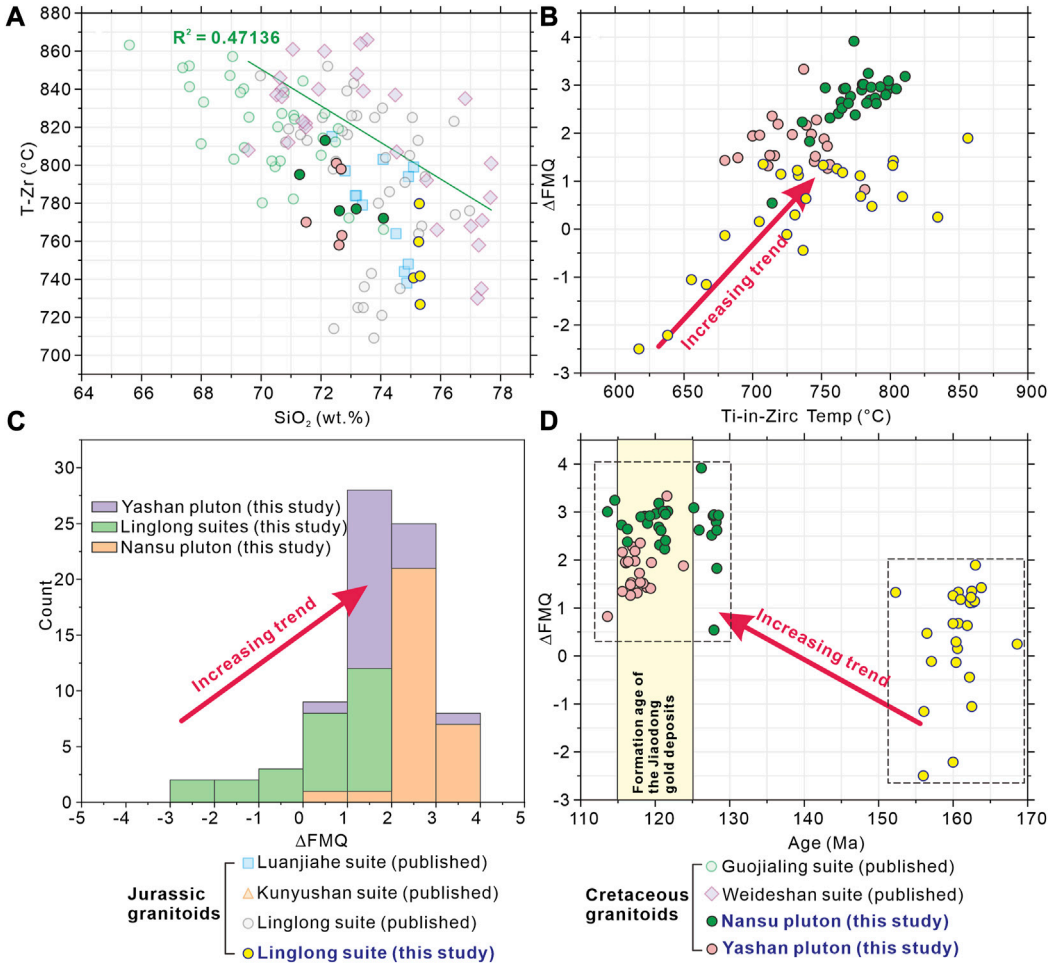

FIGURE 11
(A) Whole-rock SiO_2 (wt%) vs. T-Zr (°C); **(B)** T-Ti (°C) (Ti saturation temperature); **(C)** ΔFMQ histogram; **(D)** Age (Ma) vs. ΔFMQ. Ti saturation temperature and ΔFMQ values are calculated from zircon trace elements.

6.1.2 Evolution process of adakitic magma in Jiaodong Peninsula

The Mesozoic tectonism in the eastern NCC has been better constrained, that is, they are mainly controlled by the paleo-Pacific regime (Cai et al., 2019; Wu et al., 2019; Song et al., 2020; Cai et al., 2021; Song et al., 2021; Yang et al., 2021). As mentioned earlier, the Mesozoic granites in the Jiaodong Peninsula have the geochemical characteristics of adakitic rocks, and are derived from the partial melting of thickened lower crustal materials. Furthermore, the positive correlation between La and La/Yb and La/Sm also supports this source of partial melting of crustal materials (Figures 10A, B). However, there may be some differences between the Jurassic and Cretaceous periods. During the Middle Jurassic, the subduction of the paleo-Pacific Plate to the NCC induced the remelting of ancient continental crust materials (Dong et al., 2023a; Dong et al., 2023b), forming the Linglong granite in the Jiaodong Peninsula, which is why Linglong has a relatively low Mg# value and Co, Ni content. And the xenoliths of the ancient strata developed in the Linglong gneissic granite also prove that the continental crust is the main source area. During the Early Cretaceous, the roll-back of the paleo-Pacific Plate results in the eastern NCC being subjected to a predominantly extensional environment. Magmatism during this period appeared particularly complex, and coincided with large-scale gold mineralization events and magmatism in time. Geochemical and isotopic characteristics indicate that the Guojialing and Weideshan granites are also products of partial melting of ancient crustal materials (Figures 8C, D, 9, 10A, B), but the developed mafic microgranular enclave and moderate Mg# indicate that the formation of these granites was accompanied by mixing of mafic magma. Although there is currently no clear evidence indicating the genetic relationship between the Guojialing and Weideshan granites and gold mineralization, compared to the Jurassic magmatic evolution, the injection of mafic magma may have contributed to gold mineralization. Moreover, in the diagrams of Sr/Nd vs. Th/Yb and Nb/Y vs. Ba, the Weideshan granite has the characteristics of melt-related enrichment, which is completely different from the fluid-related enrichment shown by other plutons (Figures 10C, D). This indicates that the mafic magma during the formation of the Weideshan granite may be attributed to the partial melting of the mantle wedge that had been metasomatized by subduction slab-derived melts rather than slab-derived hydrous fluids (e.g., Ji et al., 2021).

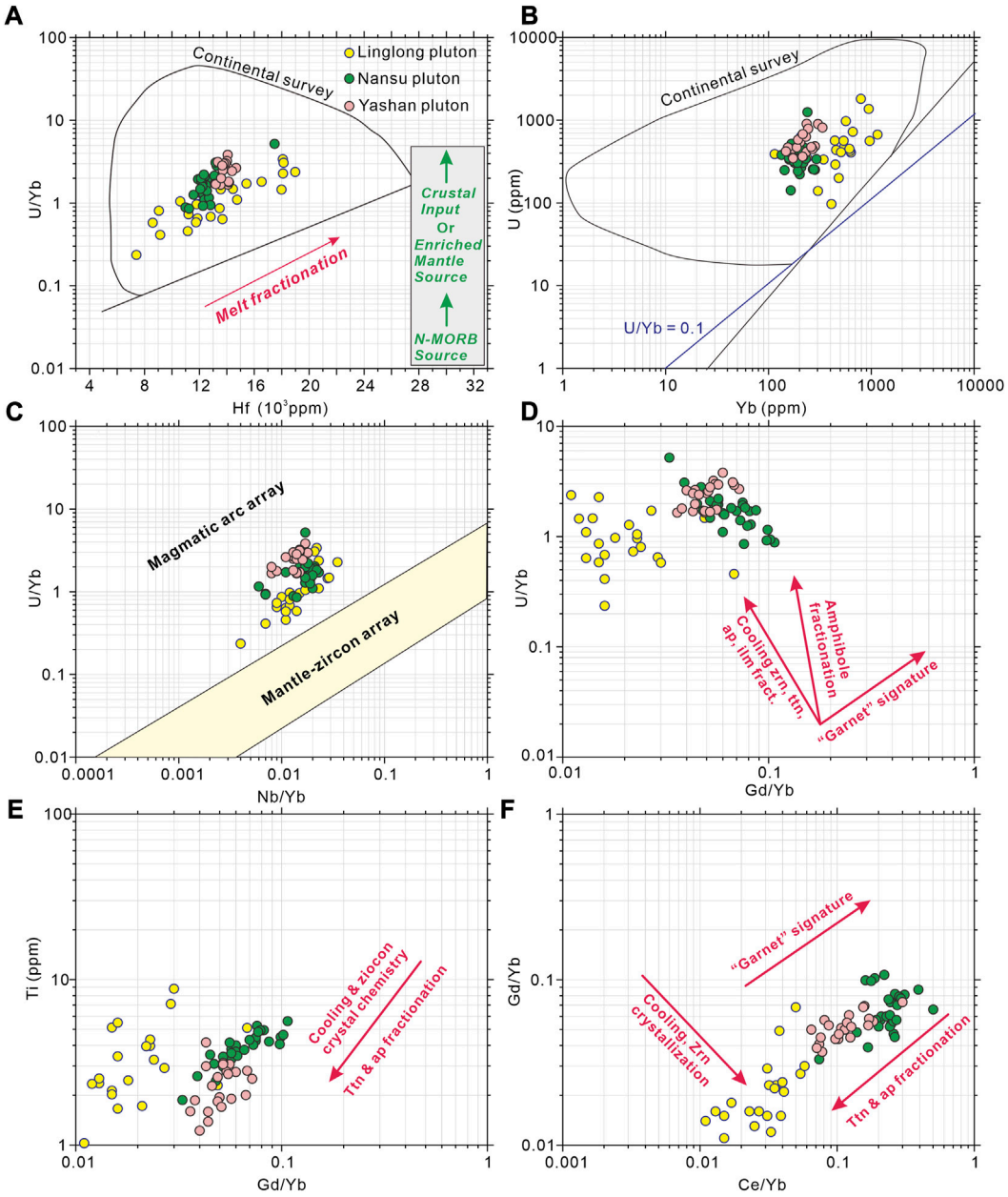

FIGURE 12
(A) Diagrams of U/Pb vs. Hf **(A)**, U vs. Yb **(B)**, U/Yb vs. Nb/Yb **(C)**, U/Yb vs. Gd/Yb **(D)**, Ti vs. Gd/Yb **(E)**, and Gd/Yb vs. Ce/Yb **(F)** (after Grimes et al., 2015), showing the zircon trace element data compiled for this study.

6.2 Magmatic physicochemical conditions

To better understand the causes of gold explosive mineralization in the Jiaodong Peninsula, a comprehensive analysis of the magmatic physicochemical conditions (e.g., oxygen fugacity and temperature) of the Jurassic Linglong granite and the Early Cretaceous Weideshan granite. The aim was to identify the key factors that restrict gold mineralization.

The zirconium saturation temperature of the Middle Jurassic granite, as revealed by the whole-rock geochemistry data (Supplementary Table S3), is between 709°C and 852°C (with an average of 758°C), which is lower than the zirconium saturation temperature of the Early Cretaceous granite (634°C–866°C, with an average of 810°C) (Figure 11A). The titanium saturation temperature shown by the zircon trace elements in this study also shows such a trend (Figure 11B), indicating that the temperature of the Middle Jurassic igneous rock is lower than that of the Early Cretaceous, which may be related to the peak thinning in the east of NCC in the Early Cretaceous. Research on porphyry mineralization systems shows a close relationship between the oxidation state of magma and mineralization (e.g., Shu et al., 2019; Cai et al., 2021). We also calculated the Linglong, Nansu, and

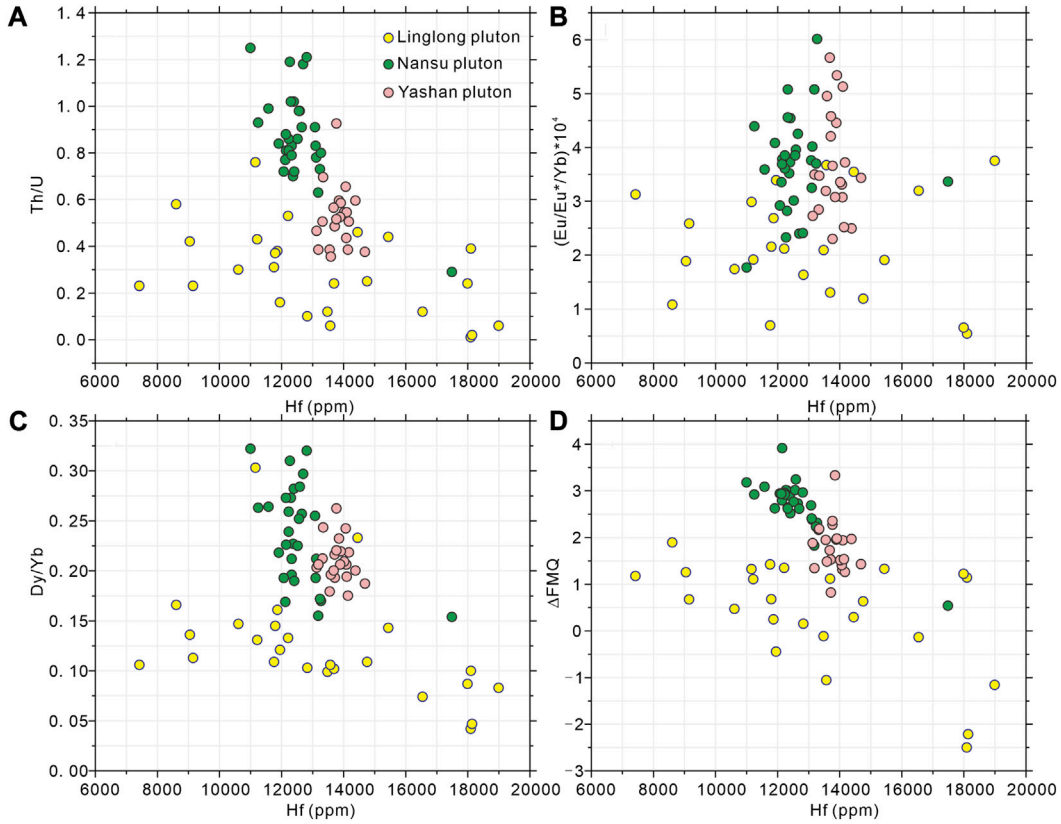

FIGURE 13
Th/U **(A)**, (Eu/Eu*)/Yb×10^4 **(B)**, Dy/Yb **(C)**, and FMQ **(D)** vs. Hf plots of zircons from the Jiaodong Peninsula Mesozoic granites.

Yashan granites based on the latest method provided by Loucks et al. (2020). This method avoids the shortcomings of the prevailing zircon oxybarometries that are subject to large analytical uncertainties of La or fractionation of minerals like titanite, plagioclase or apatite prior to zircon (Trail et al., 2012; Rezeau et al., 2019). The pressure data used in the calculation is based on the average of EPMA data of amphibole and biotite from Dong et al. (2023c). The results show that the ΔFMQ values of the Linglong suite are variable, ranging from −2.5 to +1.9, significantly lower than those of the Nansu (+0.5 to +3.9) and Yashan (+0.8 to +3.3) plutons (Figures 11C, D). This suggests that the magma in the Early Cretaceous began to become more oxidized compared to the Middle Jurassic. Previous EPMA studies on amphibole and biotite have also shown such characteristics (Dong et al., 2023c). This suggests that the high oxygen fugacity and temperature of magma in the Early Cretaceous, especially in the Weideshan suites, may be the key factors constraining gold mineralization.

6.3 Implications of Mesozoic magma for large-scale gold mineralization in Jiaodong Peninsula

The Jiaodong Peninsula contributes about 40% of China's gold resources, despite only accounting for 0.3% of its territory (Deng et al., 2020; Li et al., 2023a). This is a remarkable feat, considering that it formed in a very short duration of 5–10 million years. Therefore, the long-standing controversial issue of the Jiaodong gold deposit is how explosive mineralization in such a short duration. Previous studies have classified the attribution of Jiaodong gold deposits into orogenic (Goldfarb and Santosh, 2014), "Jiaodong" (Deng et al., 2020; Song et al., 2020), decratonic (Zhu et al., 2011; Zhu et al., 2015), or intrusion-related gold deposits (Nie et al., 2004). However, the role of magma in gold mineralization is not clear, and there is a significant spatio-temporal relationship between the Jiaodong gold deposits and the magmatic rocks (Figure 11B), regardless of the classification model. Therefore, it is possible large-scale gold mineralization have a direct or indirect relationship with magma.

The present study shows that the Middle Jurassic and Early Cretaceous granites, which are closely related to gold mineralization in temporal and spatial terms. While the Jurassic granite is only spatially related to mineralization, both types of granites share geochemical properties of adakitic rocks. It is believed that these granites were formed through partial melting of thickened lower crustal material that was associated with the subduction of the paleo-Pacific Plate. Zircon trace elements also suggest a crustal source (Figures 12A–C). There were a large number of mafic enclaves in the Early Cretaceous, indicating the mixing of mantle derived magma. However, it is unclear whether the high oxygen fugacity of Early Cretaceous magma is related to the mixing of mafic magma. Generally speaking, degassing of magma (Bell and Simon, 2011;

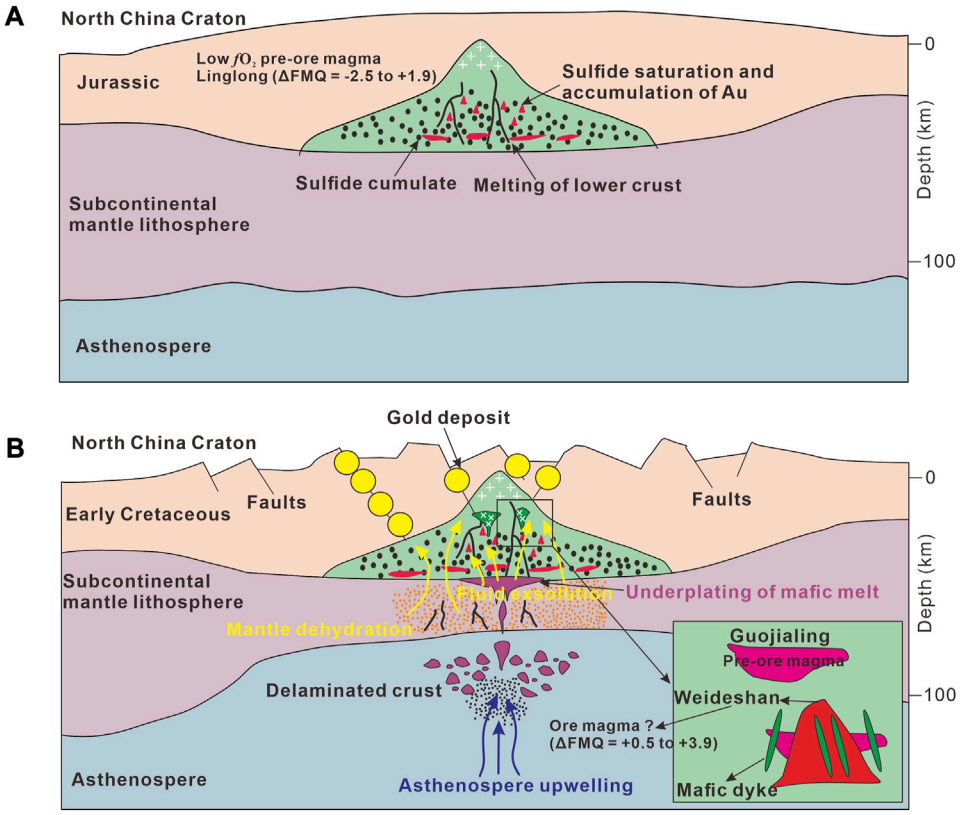

FIGURE 14
Schematic diagram of Mesozoic tectonic evolution and gold mineralization in Jiaodong Peninsula (after Dong et al., 2023c).

Moussallam et al., 2014), contamination of wallrock materials (Rowins, 2000; Li et al., 2019b), or crystallization differentiation of minerals (e.g., garnet, rutile, apatite or magnetite) (Jenner et al., 2010; Tang et al., 2018; Lee and Tang, 2020) may all cause changes in the redox state of magma. Degassing, accompanied by the escape of oxidized or reduced substances (especially sulfur and iron), usually occurs at shallow crustal levels when volatile saturation is reached, where pressures are too low to maintain high water solubility in the magma at high pressures (Baker and Alletti, 2012). Dong et al. (2023c) showed that the Guojialing suite is water unsaturated, and the Linglong granite does not contain amphibole, indicating a low water content in the pre-mineralization magma. Therefore, degassing did not play an important role in changing the oxidation states of the pre-mineralization magmas. The available data indicate that the mafic dykes contemporaneous to mineralization are also of lower water content (Liang et al., 2019). This shows that degassing is not the cause of the change in oxidation state. The present study shows that the mineralized contemporaneous Weideshan suite has a higher oxygen fugacity than the pre-mineralization magma (Figure 11), and the contemporaneous mafic dykes also show higher ΔFMQ values (Geng et al., 2019). This suggests that the mixing/injection of mafic magma favors the elevation of oxygen fugacity. The characteristic trace element ratio correlation diagram shows that there may be cooling of zircon, fractionation of apatite and rutile, and fractionation of garnet during diagenesis (Figures 12D–F). Among them, there is only a trend of garnet in the Gd/Yb vs. Ce/Yb diagram (Figure 12F), and the rare earth element composition of zircon does not show obvious LREE enrichment characteristics. Therefore, it is unlikely that the fractionation of garnet caused the change in fO_2. Crystallization of Ti-bearing minerals like ilmenite or rutile may also influence the fO_2 of magma because both of them contain Fe^{2+} (Dong et al., 2023c). Crystallization fractionation of minerals (e.g., rutile) will also cause the rise of fO_2. The diagram of zircon Hf to trace element ratios also implies significant magmatic differentiation (Figure 13).

During the Jurassic, the lower crust partially melted, forming magma with low water content and low oxygen fugacity (represented by the Linglong suite) (Figure 14A), which may have promoted the saturation and accumulation of sulfides (which may also include gold) (Dong et al., 2023c). The NCC thinning/decratonization reached a climax in the Early Cretaceous, accompanied by the upwelling of a large amount of material from the asthenosphere mantle (Figure 14B). This process may also be accompanied by the delamination of the subcontinent mantle lithosphere, forming the MME-rich Guojialing and Weideshan suites. Higher oxygen fugacity magmas of mafic magma mixed with crustal-source magmas resulted in the highest magma oxygen fugacity in the Weideshan suite (~120 Ma). The melt-related enrichment trend shown in Sr/Nd vs. Th/Yb and Nb/Y vs. Ba diagrams may also be related to this process (Figures 10C, D). Fewer contemporaneous mafic dykes are developed in the Guojialing suite (~130 Ma), suggesting that this process may not be significant. The mixed magma underwent significant fluid exsolution during upward cooling (e.g., significant crystal cave formations and pegmatites are

visible in the Aishan pluton), and the massive magma-fluid migrated sulfides and gold along the fault, and with significant changes in physicochemical conditions (temperature and pressure reduction), the migrated gold complexes (e.g., $Au(HS)^0$, $Au(HS)^{2-}$) (Williams-Jones et al., 2009) destabilized and formed massive gold ore bodies within the fault (Figure 14B). This model provides insights into the explosive and instantaneous mineralization of the Jiaodong gold deposit, suggesting that it may differ from the traditional orogenic gold deposit category (Groves et al., 1998).

7 Conclusion

The Mesozoic (Middle Jurassic and Early Cretaceous) granites of the Jiaodong Peninsula exhibit geochemical signatures of adakitic rocks and are derived from partial melting of the thickened lower crust associated with the subduction of the paleo-Pacific Plate. The addition of mantle materials is also observed in the Early Cretaceous magmatic rocks. The pre-ore magmas (Linglong granites) have relatively low oxygen fugacity, while the Weideshan granites during the mineralization period have the highest oxygen fugacity due to mixing with oxidized mafic magmas. Our model suggests that the low oxygen fugacity pre-ore magma promoted the accumulation of sulfides, and the upwelling of crust-mantle mixed oxidized magma in the Early Cretaceous (Weideshan suites) allowed a large amount of sulfides and gold to be migrated and mineralized at the fault site. This model provides an explanation for the transient and explosive gold mineralization in the Jiaodong Peninsula.

Data availability statement

The original contributions presented in the study are included in the article/Supplementary Material, further inquiries can be directed to the corresponding author.

Author contributions

All authors listed have made a substantial, direct, and intellectual contribution to the work and approved it for publication.

Funding

This work was financially supported by the National Natural Science Foundation of China-Shandong Joint Fund (No. U2006201) and Shandong Natural Science Foundation (No. ZR2021QD056).

Acknowledgments

We gratefully acknowledge the Associate Editor Fan Yang and three reviewers for their insightful comments, which greatly improved the manuscript.

Conflict of interest

Authors JL, C-WW, and C-JW were employed by Shandong Zhengyuan Geological Resources Exploration Co.,Ltd. Authors C-GD, H-JS, K-LX, and PW were employed by Shandong Province Nuclear Industry Geological Group 273.

The remaining authors declare that the research was conducted in the absence of any commercial or financial relationships that could be construed as a potential conflict of interest.

Publisher's note

Supplementary material

The Supplementary Material for this article can be found online at: https://www.frontiersin.org/articles/10.3389/feart.2023.1243844/full#supplementary-material

SUPPLEMENTARY FIGURE S1
Representative photos show that the orebody occurs in Mesozoic granite.

References

Andersen, T. (2002). Correction of common lead in U–Pb analyses that do not report ^{204}Pb. *Chem. Geol.* 192, 59–79. doi:10.1016/s0009-2541(02)00195-x

Atherton, M. P., and Petford, N. (1993). Generation of sodium-rich magmas from newly underplated basaltic crust. *Nature* 362, 144–146. doi:10.1038/362144a0

Baker, D. R., and Alletti, M. (2012). Fluid saturation and volatile partitioning between melts and hydrous fluids in crustal magmatic systems: the contribution of experimental measurements and solubility models. *Earth Sci. Rev.* 114, 298–324. doi:10.1016/j.earscirev.2012.06.005

Bell, A. S., and Simon, A. (2011). Experimental evidence for the alteration of the $Fe^{3+}/\Sigma Fe$ of silicate melt caused by the degassing of chlorine-bearing aqueous volatiles. *Geology* 39, 499–502. doi:10.1130/g31828.1

Cai, W. Y., Wang, Z. G., Li, J., Fu, L. J., Wang, K. Y., Yasssa, K., et al. (2019). Zircon U–Pb and molybdenite Re–Os geochronology and geochemistry of jinchang porphyry gold–copper deposit, NE China: two-phase mineralization and the tectonic setting. *Ore Geol. Rev.* 107, 735–753. doi:10.1016/j.oregeorev.2019.03.018

Cai, W. Y., Wang, K. Y., Li, J., Fu, L. J., Lai, C. K., and Liu, H. L. (2021). Geology, geochronology and geochemistry of large Duobaoshan Cu–Mo–Au orefield in NE China: magma genesis and regional tectonic implications. *Geosci. Front.* 12, 265–292. doi:10.1016/j.gsf.2020.04.013

Castillo, P. R., Janney, P. E., and Solidum, R. U. (1999). Petrology and geochemistry of Camiguin Island, southern Philippines: insights to the source of adakites and other lavas in a complex arc setting. *Contribution Mineralogy Petrology* 134, 33–51. doi:10.1007/s004100050467

Defant, M. J., and Drummond, M. S. (1990). Derivation of some modern arc magmas by melting of young subducted lithosphere. *Nature* 347, 662–665. doi:10.1038/347662a0

Defant, M. J., Xu, J. F., Kepezhinskas, P., Wang, Q., Zhang, Q., and Xiao, L. (2002). Adakites: some variations on a theme. *Acta Petrol. Sin.* 18, 129–142.

Deng, J., Yang, L. Q., Groves, D. I., Zhang, L., Qiu, K. F., and Wang, Q. F. (2020). An integrated mineral system model for the gold deposits of the giant Jiaodong province, eastern China. *Earth-Science Rev.* 208, 103274. doi:10.1016/j.earscirev.2020.103274

Dong, L. L., Yang, Z. M., Song, M. C., and Bai, X. (2023a). *Petrogenesis of mesozoic magmatic suites in the Jiaodong peninsula: implications for crust-mantle interactions and decratonization*. Lithosphere 6226908.

Dong, L. L., Yang, Z. M., Bai, X., and Deng, C. (2023b). Generation of the early cretaceous granitoid in the dazeshan region, Jiaodong peninsula: implications for the crustal reworking in the north China craton. *Front. Earth Sci.* 10, 1083608. doi:10.3389/feart.2022.1083608

Dong, L. L., Yang, Z. M., Liu, Y. H., and Song, M. C. (2023c). Possible source of Au in the Jiaodong area from lower crustal sulfide cumulates: evidence from oxygen states and chalcophile elements contents of Mesozoic magmatic suites. *Ore Geol. Rev.* 153, 105268. doi:10.1016/j.oregeorev.2022.105268

Drummond, M. S., Defant, M. J., and Kepezhinskas, P. K. (1996). "Petrogenesis of slab-derived trondhjemite–tonalite–dacite/adakite magmas,". *Third hutton symposium on the origin of granites and related rocks, special paper*. Editors M. Brown, P. A. Candela, and D. L. Pecket (Boulder, CO: Geological Society of America), 315, 205–215.

Fan, H. R., Feng, K., Li, X. H., Hu, F. F., and Yang, K. F. (2016). Mesozoic gold mineralization in the Jiaodong and Korean peninsulas. *Acta Petrol. Sin.* 32, 3225–3238. (in Chinese with English abstract).

Gao, S., Rudnick, R. L., Carlson, R. W., McDonough, W. F., and Liu, Y. S. (2002). Re–Os evidence for replacement of ancient mantle lithosphere beneath the North China Craton. *Earth Planet. Sci. Lett.* 198, 307–322. doi:10.1016/s0012-821x(02)00489-2

Geng, X., Foley, S. F., Liu, Y., Wang, Z., Hu, Z., and Zhou, L. (2019). Thermal-chemical conditions of the North China Mesozoic lithospheric mantle and implication for the lithospheric thinning of cratons. *Earth Planet. Sci. Lett.* 516, 1–11. doi:10.1016/j.epsl.2019.03.012

Goldfarb, R. J., and Santosh, M. (2014). The dilemma of the Jiaodong gold deposits: are they unique? *Geosci. Front.* 5, 139–153. doi:10.1016/j.gsf.2013.11.001

Goss, S. C., Wilde, S. A., Wu, F., and Yang, J. (2010). The age, isotopic signature and significance of the youngest mesozoic granitoids in the Jiaodong terrane, Shandong province, north China craton. *Lithos* 120, 309–326. doi:10.1016/j.lithos.2010.08.019

Griffin, W. L., Zhang, A., O'Reilly, S. Y., and Ryan, C. G. (1998). "Phanerozoic evolution of the lithosphere beneath the sino-Korean craton,". *Mantle dynamics and plate interactions in east Asia, geodynamics series*. Editors M. F. J. Flower, S.-L. Chung, C.-H. Lo, and T.-Y. Lee (Washington DC: American Geophysical Union), 27, 107–126. doi:10.1029/GD027p0107

Grimes, C. B., John, B. E., Cheadle, J. L., and John, B. E. (2015). "Fingerprinting" tectono-magmatic provenance using trace elements in igneous zircon. *Contributions Mineralogy Petrology* 170, 1–26. doi:10.1007/s00410-015-1199-3

Groves, D. I., Goldfarb, R. J., Gebre-Mariam, M., Hagemann, S. G., and Robert, F. (1998). Orogenic gold deposits: a proposed classification in the context of their crustal distribution and relationship to other gold deposit types. *Ore Geol. Rev.* 13, 7–27. doi:10.1016/s0169-1368(97)00012-7

Hart, C. G. R., Goldfarb, R. J., Qiu, Y. M., Snee, L., Miller, L. D., and Miller, M. L. (2002). Gold deposits of the northern margin of the north China craton: multiple late PaleozoicMesozoic mineralizing events. *Mineral. Deposita* 37, 326–351. doi:10.1007/s00126-001-0239-2

He, J. T. (2021). *Gold mineralization and post ore enrollment in the muping rushan gold Belt, Jiaodong peninsula, eastern China*. Ph.D. thesis. Beiijing: china University of Geosciences, 1–171. (in Chinese with English abstract).

Hofmann, A. W., Jochum, K. P., Seufert, M., and White, W. M. (1986). Nb and Pb in oceanicbasalts: new constraints on mantle evolution. *Earth Planet Sci. Lett.* 79, 33–45. doi:10.1016/0012-821x(86)90038-5

Hoskin, P. W. O., and Black, L. P. (2000). Metamorphic zircon formation by solid-state recrystallization of protolith igneous zircon. *J. Metamorph. Geol.* 18, 423–439. doi:10.1046/j.1525-1314.2000.00266.x

Hoskin, P. W. O. (2005). Trace-element composition of hydrothermal zircon and the alteration of hadean zircon from the Jack Hills, Australia. *Geochimica Cosmochimica Acta* 69, 637–648. doi:10.1016/j.gca.2004.07.006

Hou, M. L., Jiang, Y. H., Jiang, S. Y., Ling, H. F., and Zhao, K. D. (2007). Contrasting origins of late mesozoic adakitic granitoids from the northwestern,Jiaodong Peninsula, east China: implications for crustal thickening to delamination. *Geol. Mag.* 144, 619–631. doi:10.1017/s0016756807003494

Irvine, T. H., and Baragar, W. R. A. (1971). A guide to the chemical classification of the common volcanic rocks. *Can. J. Earth Sci.* 8, 523–548. doi:10.1139/e71-055

Jenner, F. E., O'Neill, H. S. C., Arculus, R. J., and Mavrogenes, J. A. (2010). The magnetite crisis in the evolution of arc-related magmas and the initial concentration of Au, Ag and Cu. *J. Petrol.* 51, 2445–2464. doi:10.1093/petrology/egq063

Ji, Z., Ge, W. C., He, Y., Bi, J. H., Dong, Y., Yang, H., et al. (2021). Mixing of cognate magmas as a process for producing high-silica granites: insights from Guanmenshan Complex in Liaodong Peninsula, China. *Lithos* 406–407, 106495. doi:10.1016/j.lithos.2021.106495

Jiang, P., Yang, K. F., Fan, H. R., Liu, X., Cai, Y. C., and Yang, Y. H. (2016). Titanite-scale insights into multi-stage magma mixing in early cretaceous of NW Jiaodong terrane, north China craton. *Lithos* 258–259, 197–214. doi:10.1016/j.lithos.2016.04.028

Kepezhinskas, P., McDermott, F., Defant, M. J., Hochstaedter, A., Drummond, M. S., Hawkesworth, C. J., et al. (1997). Trace element and Sr Nd-Pb isotopic constraints on a three-component model of Kamchatka Arc petrogenesis. *Geochim. Cosmochim. Acta* 61, 577–600. doi:10.1016/s0016-7037(96)00349-3

Lee, C. T. A., and Tang, M. (2020). How to make porphyry copper deposits. *Earth Planet. Sci. Lett.* 529, 115868. doi:10.1016/j.epsl.2019.115868

Li, X. C., Fan, H. R., Santosh, M., Hu, F. F., Yang, K. F., Lan, T. G., et al. (2012). An evolving magma chamber within extending lithosphere: an integrated geochemical, isotopic and zircon U-Pb geochronological study of the Gushan granite, eastern North China Craton. *J. Asian Earth Sci.* 50, 27–43. doi:10.1016/j.jseaes.2012.01.016

Li, J., Cai, W. Y., Li, B., Wang, K. Y., Liu, H. L., Yassa, K., et al. (2019a). Paleoproterozoic SEDEX-type stratiform mineralization overprinted by Mesozoic vein-type mineralization in the Qingchengzi Pb-Zn deposit, Northeastern China. *J. Asian Earth Sci.* 184, 104009. doi:10.1016/j.jseaes.2019.104009

Li, X. H., Fan, H. R., Hu, F. F., Hollings, P., Yang, K. F., and Liu, X. (2019b). Linking lithospheric thinning and magmatic evolution of late jurassic to early cretaceous granitoids in the jiaobei terrane, southeastern north China craton. *Lithos* 324–325, 280–296. doi:10.1016/j.lithos.2018.11.022

Li, J., Cai, W. Y., Wang, K. Y., Kim, N. H., Liu, H. L., Lee, J. G., et al. (2020a). Initial decratonization of the eastern North China Craton: new constraints from geochronology, geochemistry, and Hf isotopic compositions of Mesozoic igneous rocks in the Qingchengzi district. *Geol. J.* 55, 3796–3820. doi:10.1002/gj.3635

Li, J., Wang, K. Y., Cai, W. Y., Sun, F. Y., Liu, H. L., Fu, L. J., et al. (2020b). Triassic gold-silver metallogenesis in Qingchengzi orefield, North China Craton: perspective from fluid inclusions, REE and H-O-S-Pb isotope systematics. *Ore Geol. Rev.* 121, 103567. doi:10.1016/j.oregeorev.2020.103567

Li, J., Song, M. C., Yu, J. T., Bo, J. W., Zhang, Z. L., and Liu, X. (2022). Genesis of Jinqingding Gold Deposit in eastern Jiaodong peninsula, China: constrain from trace elements of sulfide ore and wall-rock. *Geol. Bull. China* 41, 1010–1022. (in Chinese with English abstract). doi:10.12097/i.issn.1671-2552.2022.06.009

Li, J., Yang, Z. M., Song, M. C., Dong, L. L., Li, S. Y., Wang, R. S., et al. (2023a). Gold remobilization of the Sanshandao gold deposit, Jiaodong Peninsula, Eastern China: perspective from *in-situ* sulfide trace elements and sulfur isotopes. *Ore Geol. Rev.* 158, 105505. doi:10.1016/j.oregeorev.2023.105505

Li, J., Yang, Z. M., Wang, C. W., Chu, Z. B., Liu, X., Cui, Q. Y., et al. (2023b). Metallogeny of the Xiaotongjiapuzi gold deposit, Liaodong Peninsula (Eastern China): perspective from sulfide trace element geochemistry and sulfur isotopes. *Ore Geol. Rev.* 157, 105455. doi:10.1016/j.oregeorev.2023.105455

Liang, Y., Deng, J., Liu, X., Wang, Q., Ma, Y., Gao, T., et al. (2019). Water contents of early cretaceous mafic dikes in the Jiaodong peninsula, eastern north China craton: insights into an enriched lithospheric mantle source metasomatized by PaleoPacific plate subduction-related fluids. *J. Geol.* 127, 343–362. doi:10.1086/702648

Liu, D. Y., Nutman, A. P., Compston, W., Wu, J. S., and Shen, Q. H. (1992). Remnants of ≥3800 Ma crust in the Chinese part of the SinoKorean craton. *Geology* 20, 339–342. doi:10.1130/0091-7613(1992)020<0339:romcit>2.3.co;2

Loucks, R. R., Fiorentini, M. L., and Henríquez, G. J. (2020). New magmatic oxybarometer using trace elements in zircon. *J. Petrol.* 61, egaa034. doi:10.1093/petrology/egaa034

Ludwig, K. R. (2003). *User's manual for isoplot 3.0: A geochronological toolkit for microsoft excel*. Berkeley: Berkeley Geochronology Center Special Publication 4, 25–32.

Ma, L., Jiang, S. Y., Dai, B. Z., Jiang, Y. H., Hou, M. L., Pu, W., et al. (2013). Multiple sources for the origin of late jurassic Linglong adakitic granite in the Shandong peninsula, eastern China: zircon U-Pb geochronological geochemical and Sr-Nd-Hf isotopic evidence. *Lithos* 162, 251–263. doi:10.1016/j.lithos.2013.01.009

Ma, L., Jiang, S. Y., Hou, M. L., Dai, B. Z., Jiang, Y. H., Yang, T., et al. (2014). Geochemistry of early cretaceous calc-alkaline lamprophyres in the Jiaodong peninsula: implication for lithospheric evolution of the eastern north China craton. *Gondwana Res.* 25, 859–872. doi:10.1016/j.gr.2013.05.012

Macpherson, C. G., Dreher, S. T., and Thirlwall, M. F. (2006). Adakites without slab melting: high pressure differentiation of island arc magma, Mindanao, the Philippines. *Earth Planet. Sci. Lett.* 243, 581–593. doi:10.1016/j.epsl.2005.12.034

Maniar, P. D., and Piccoli, P. M. (1989). Tectonic discrimination of granitoids. *Geol. Soc. Am. Bull.* 101, 635–643. doi:10.1130/0016-7606(1989)101<0635:tdog>2.3.co;2

Martin, H., Smithies, R. H., Rapp, R., Moyen, J. F., and Champion, D. C. (2005). An overview of adakite, tonalite–trondhjemite–granodiorite (TTG), and sanukitoid: relationships and some implications for crustal evolution. *Lithos* 79, 1–24. doi:10.1016/j.lithos.2004.04.048

Martin, H. (1986). Effect of steeper Archean geothermal gradient on geochemistry of subduction-zone magmas. *Geology* 14, 753–756. doi:10.1130/0091-7613(1986)14<753:eosagg>2.0.co;2

Martin, H. (1987). Petrogenesis of archaean trondhjemites, tonalites, and granodiorites from eastern Finland: major and trace element geochemistry. *J. Petrol.* 28, 921–953. doi:10.1093/petrology/28.5.921

Martin, H. (1999). Adakitic magmas: modern analogues of archaean granitoids. *Lithos* 46, 411–429. doi:10.1016/s0024-4937(98)00076-0

McDonough, W. F., and Sun, S. S. (1995). The composition of the Earth. *Chem. Geol.* 120, 223–253. doi:10.1016/0009-2541(94)00140-4

Menzies, M. A., Fan, W., and Zhang, M. (1993). Palaeozoic and Cenozoic lithoprobes and the loss of >120 km of Archaean lithosphere, Sino-Korean craton, China. *Magmatic Process. Plate Tect.* 76, 71–81. doi:10.1144/gsl.sp.1993.076.01.04

Moussallam, Y., Oppenheimer, C., Scaillet, B., Gaillard, F., Kyle, P. R., Peters, N., et al. (2014). Tracking the changing oxidation state of Erebus magmas, from mantle to surface, driven by magma ascent and degassing. *Earth Planet. Sci. Lett.* 393, 200–209. doi:10.1016/j.epsl.2014.02.055

Moyen, J. F. (2009). High Sr/Y and La/Yb ratios: the meaning of the "adakitic signature". *Lithos* 112, 556–574. doi:10.1016/j.lithos.2009.04.001

Nie, F. J., Jiang, S. H., and Liu, Y. (2004). Intrusion-related gold deposits of north China craton, people's Republic of China. *Resour. Geol.* 54, 299–324. doi:10.1111/j.1751-3928.2004.tb00208.x

Paton, C., Woodhead, J. D., Hellstrom, J. C., Hergt, J. M., Greig, A., and Maas, R. (2010). Improved laser ablation U-Pb zircon geochronology through robust downhole fractionation correction. *Geochem. Geophys. Geosystems* 11, Q0AA06. doi:10.1029/2009gc002618

Pearce, J. A. (1983). "Role of the sub-continental lithosphere in magma genesis at active continental margins," in *Continental basalts and mantle xenoliths*. Editors C. J. Hawkesworth and M. J. Norry (Nantwich: Shiva Press), 230–249.

Peccerillo, A., and Taylor, D. R. (1976). Geochemistry of Eocene calc-alkaline volcanic rocks from the Kastamonu area, northern Turkey. *Contributions Mineralogy Petrology* 58, 63–81. doi:10.1007/bf00384745

Rezeau, H., Moritz, R., Wotzlaw, J. F., Hovakimyan, S., and Tayan, R. (2019). Zircon petrochronology of the meghri-ordubad pluton, lesser caucasus: fingerprinting igneous processes and implications for the exploration of porphyry Cu-Mo deposits. *Econ. Geol.* 114, 1365–1388. doi:10.5382/econgeo.4671

Richards, J. P., and Kerrich, R. (2007). Special paper: adakite-like rocks: their diverse origins and questionable role in metallogenesis. *Econ. Geol.* 102, 537–576. doi:10.2113/gsecongeo.102.4.537

Rowins, S. M. (2000). Reduced porphyry copper-gold deposits: a new variation on an old theme. *Geology* 28, 491–494. doi:10.1130/0091-7613(2000)028<0491:rpcgda>2.3.co;2

Rubatto, D., and Gebauer, D. (2000). "Use of cathodoluminescence for U-Pb Zircon dating by ion microprobe. Some examples from the western Alps," in *Cathodoluminescence in Geosciences*. Editors M. Pagel, V. Barbin, P. Blanc, and D. Ohnenstetter (Berlin, Heidelberg: Springer), 373–400.

Rudnick, R. L., Gao, S., Ling, W. L., Liu, Y. S., and McDonough, W. F. (2004). Petrology and geochemistry of spinel peridotite xenoliths from hannuoba and Qixia, north China craton. *Lithos* 77, 609–637. doi:10.1016/j.lithos.2004.03.033

Santosh, M. (2010). Assembling North China craton within the columbia supercontinent: the role of double-sided subduction. *Precambr. Res.* 178, 149–167. doi:10.1016/j.precamres.2010.02.003

Shu, Q. H., Chang, Z. S., Lai, Y., Hu, X. L., Wu, H. Y., Zhang, Y., et al. (2019). Zircon trace elements and magma fertility: insights from porphyry (-skarn) Mo deposits in NE China. *Min. Deposita* 54, 645–656. doi:10.1007/s00126-019-00867-7

Smithies, R. H. (2000). The Archaean tonalite–trondhjemite–granodiorite (TTG) series is not an analogue of Cenozoic adakite. *Earth Planet. Sci. Lett.* 182, 115–125. doi:10.1016/s0012-821x(00)00236-3

Song, M. C., Song, Y. X., Ding, Z. J., and Li, S. Y. (2018). Jiaodong gold deposits: essential characteristics and major controversy. *Gold Sci. Technol.* 26, 406–422. (in Chinese with English abstract). doi:10.11872/j.issn.1005-2518.2018.04.406

Song, M. C., Zhou, J. B., Song, Y. X., Wang, B., Li, S,Y., Li, J., et al. (2020). Mesozoic Weideshan granitoid suite and its relationship to large-scale gold mineralization in the Jiaodong Peninsula, China. *Geol. J.* 55, 5703–5724. doi:10.1002/gj.3607

Song, M. C., Li, J., Yu, X. F., Ding, Z. J., and Li, S. Y. (2021). Metallogenic characteristics and tectonic setting of the Jiaodong gold deposit, China. *Solid Earth Sci.* 6, 385–405. doi:10.1016/j.sesci.2021.07.002

Stern, C. R., and Kilian, R. (1996). Role of the subducted slab, mantle wedge and continental crust in the generation of adakites from the Andean Austral Volcanic Zone. *Contributions Mineralogy Petrology* 123, 263–281. doi:10.1007/s004100050155

Stevenson, R. K., David, J., and Parent, M. (2006). Crustal evolution of the western minto block, northern superior province, Canada. *Precambrian Res.* 145, 229–242. doi:10.1016/j.precamres.2005.12.004

Tang, M., Erdman, M., Eldridge, G., and Lee, C. T. A. (2018). The redox "filter" beneath magmatic orogens and the formation of continental crust. *Sci. Adv.* 4, eaar4444. doi:10.1126/sciadv.aar4444

Taylor, S. R., and McLennan, S. M. (1985). *The continental crust: Its composition andEvolution*. Blackwell: Oxford Press, 312.

Tischendorf, G., and Paelchen, W. (1985). On the classification of granitoids. *Z. Fuer Geol. Wiss.* 13, 615–627.

Trail, D., Bruce Watson, E., and Tailby, N. D. (2012). Ce and Eu anomalies in zircon as proxies for the oxidation state of magmas. *Geochim. Cosmochim. Acta* 97, 70–87. doi:10.1016/j.gca.2012.08.032

Wang, B., Song, M. C., Huo, G., Zhou, M. L., Xu, Z. H., Jiang, L., et al. (2021). Risk factors associated with deep vein thrombosis in COVID-19 patients. *Acta Petrologica Mineralogica* 40, 288–291. (in Chinese with English abstract). doi:10.1002/mco2.52

Wang, B., Ding, Z., Bao, Z., Song, M., Zhou, J., Lv, J., et al. (2022). Mesozoic magmatic and geodynamic evolution in the Jiaodong peninsula, China: implications for the gold and polymetallic mineralization. *Minerals* 12, 1073. doi:10.3390/min12091073

Wang, D., Wang, T. Q., and Li, H. Y. (2023). Petrogenesis of early cretaceous laoshan A-type granites and the implications for the tectonic evolution of Jiaodong peninsula. *Acta Petrol. Sin.* 39, 317–339. (in Chinese with English abstract). doi:10.18654/1000-0569/2023.02.03

Williams-Jones, A. E., Bowell, R. J., and Migdisov, A. A. (2009). Gold in solution. *Elements* 5, 281–287. doi:10.2113/gselements.5.5.281

Wilson, M. (1989). *Igneous petrogenesis a global tectonic approach*. London: London Unwin Hyman, 466.

Woodhead, J. D., Eggins, S. M., and Johnson, R. W. (1998). Magma genesis in the new britain island arc: further insights into melting and mass transfer processes. *J. Petrol.* 39, 1641–1668. doi:10.1093/petroj/39.9.1641

Wu, F. Y., Xu, Y. G., Gao, S., and Zheng, J. P. (2008). Lithospheric thinning and destruction of the north China craton. *Acta Petrol. Sin.* 24, 1145–1174. (in Chinese with English abstract).

Wu, F. Y., Yang, J. H., Xu, Y. G., Wilde, S. A., and Walker, R. J. (2019). Destruction of the north China craton in the mesozoic. *Annu. Rev. Earth Planet. Sci.* 47, 173–195. doi:10.1146/annurev-earth-053018-060342

Xu, J. F., Shinjo, R., Defant, M. J., Wang, Q., and Papp, R. P. (2002). Origin of Mesozoic adakitic intrusive rock in the Ningzhen area of east China: partial melting of delaminated lower continental crust? *Geology* 30, 1111–1114. doi:10.1130/0091-7613(2002)030<1111:oomair>2.0.co;2

Yang, K. F., Fan, H. R., Santosh, M., Hu, F. F., Wilde, S., Lan, T. G., et al. (2012). Reactivation of the archean lower crust: implications for zircon geochronology, elemental and Sr–Nd–Hf isotopic geochemistry of late mesozoic granitoids from northwestern Jiaodong terrane, the north China craton. *Lithos* 146, 112–127. doi:10.1016/j.lithos.2012.04.035

Yang, L. Q., Deng, J., Wang, Z. L., Zhang, L., Guo, L. N., Song, M. C., et al. (2014). Mesozoic gold metallogenic system of the Jiaodong gold province, eastern China. *Acta Petrol. Sin.* 30, 2447–2467. (in Chinese with English abstract).

Yang, L. Q., Dilek, Y., Wang, Z. L., Weinberg, R. F., and Liu, Y. (2017). Late Jurassic, high Ba–Sr Linglong granites in the Jiaodong Peninsula, east China: lower crustal melting products in the eastern north China craton. *Geol. Mag.* 155, 1040–1062. doi:10.1017/s0016756816001230

Yang, F., Santosh, M., and Kim, S. W. (2018). Mesozoic magmatism in the eastern North China Craton: insights on tectonic cycles associated with progressive craton destruction. *Gondwana Res.* 60, 153–178. doi:10.1016/j.gr.2018.04.003

Yang, F., Santosh, M., Glorie, S., Jepson, G., Xue, F., and Kim, S. W. (2020). Meso-cenozoic multiple exhumation in the Shandong peninsula, eastern north China craton: implications for lithospheric destruction. *Lithos* 370–371, 105597. doi:10.1016/j.lithos.2020.105597

Yang, J. H., Xu, L., Sun, J. F., Zeng, Q. D., Zhao, Y. N., Wang, H., et al. (2021). Geodynamics of decratonization and related magmatism and mineralization in the North China Craton. *Sci. China-Earth Sci.* 64, 1409–1427. doi:10.1007/s11430-020-9732-6

Zhang, L., Weinberg, R. F., Yang, L. Q., Groves, D. I., Sai, S. X., Matchan, E., et al. (2020). Mesozoic orogenic gold mineralization in the Jiaodong peninsula, China: a focused event at 120 ± 2 Ma during cooling of pre-gold granite intrusions. *Econ. Geol.* 115, 415–441. doi:10.5382/econgeo.4716

Zhao, G. C., and Zhai, M. G. (2013). Lithotectonic elements of precambrian basement in the north China craton: review and tectonic implications. *Gondwana Res.* 23, 1207–1240. doi:10.1016/j.gr.2012.08.016

Zhao, G. C., Wilde, S. A., Cawood, P. A., and Sun, M. (2001). Archean blocks and their boundaries in the north China craton: lithological, geochemical, structural and P-T, path constraints and tectonic evolution. *Precambr. Res.* 107, 45–73. doi:10.1016/s0301-9268(00)00154-6

Zhao, G. C., Sun, M., Wilde, S. A., and Li, S. Z. (2005). Late archean to paleoproterozoic evolution of the north China craton: key issues revisited. *Precambrian Res.* 136, 177–202. doi:10.1016/j.precamres.2004.10.002

Zhong, S., Seltmann, R., Qu, H., and Song, Y. (2019). Characterization of the zircon Ce anomaly for estimation of oxidation state of magmas: a revised Ce/Ce* method. *Mineral. Petrol.* 113, 755–763. doi:10.1007/s00710-019-00682-y

Zhu, R. X., Chen, L., Wu, F. Y., and Liu, J. L. (2011). Timing, scale and mechanism of the destruction of the North China Craton. *Sci. China-Earth Sci.* 54, 789–797. doi:10.1007/s11430-011-4203-4

Zhu, R. X., Fan, H. R., Li, J. W., Meng, Q. R., Li, S. R., and Zeng, Q. D. (2015). Decratonic gold deposits. *Sci. China-Earth Sci.* 58, 1523–1537. doi:10.1007/s11430-015-5139-x